

With respect to the Secondary Sodium Leak Accident that occurred on December 8, 1995, out-of-pile reproduction experiments were carried out to investigate the cause of the accident and prevent its recurrence (Photo 4-1). The experimental results were reflected to validation and advancement of the ASSCOPS models. Furthermore, the mechanisms of steel floor liner corrosion due to chemical reactions with leaking sodium were investigated and elucidated. The safety evaluation of the accident was revised based on new findings that a rapidly proceeding mechanism of “molten salt type corrosion” may occur theoretically even though such a corrosion mechanism is unlikely to occur under actual conditions in Monju.

An evaluation of thermal effects of intermediate- and small-scale sodium leak confirmed that the steel liner would not be penetrated if the amount of leaking sodium was limited by emergency sodium drain, even when assuming a conservative corrosion rate of the liner, and thereby contact between sodium and concrete was prevented. In addition, for a large-scale sodium leak, it was confirmed that the integrity of building concrete would be maintained against the increase in pressure and temperature during leak from a break opening with an area of $Dt/4$. Namely, it was confirmed that the integrity of the reactor auxiliary building would not be impaired by the thermal effects of leaking sodium and that the separation between cooling systems would be maintained.

(4) SG tube rupture accident

When a heat transfer tube rupture occurs in the SG, sodium-water reaction causes large pressure increase and the water leak would be detected by cover gas pressure gauge installed in evaporators in order to prevent and mitigate the escalation to a large-scale water leak. This water leak signal activates a series of automatic plant shutdown operations, including rapid discharge (blow) of water and steam retained in the SGs.

Concerning the sodium-water reaction, experimental studies were performed under various scales and conditions of water leak to obtain the following achievements: clarification of the mechanism of adjacent tube failure (wastage-type failure is dominant); development of an analysis code to evaluate the initial spike pressure and quasi-stationary pressure; setting of the upper limit of the scale of water leak to be postulated as a design basis leak (equivalent to one tube plus three adjacent tubes: one tube for the evaluation of the initial spike pressure, and four tubes for the evaluation of quasi-stationary

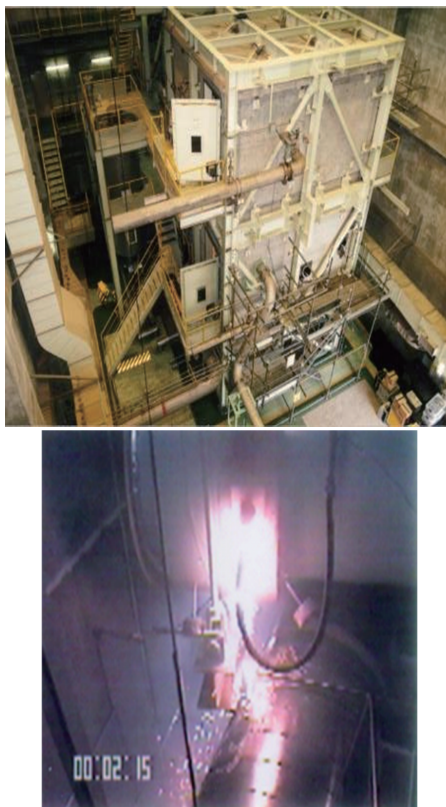


Photo 4-1 Experiment to reproduce the Sodium Leak Accident and sodium burning behavior

pressure). Accident analyses based on these data confirmed the design validity of water leak detectors and equipment for mitigating the effect of sodium-water reactions.

The possibility of high-temperature rupture type failure propagation was examined in consideration of the accident that occurred in the U.K. Prototype Fast Reactor (PFR) in 1987, in which many heat transport tubes failed almost simultaneously (the direct cause was that the PFR's superheater was not equipped with a rapid steam blow system, which was installed in Monju). An experiment simulating the occurrence conditions of high-temperature rupture (see 4.6.3) and a quantitative evaluation thereof confirmed that the possibility of high-temperature rupture type failure propagation could be virtually eliminated in Monju.

(5) Local faults

FR fuel subassemblies are characterized by: fuel pins arranged in a regular-triangle lattice, high power density, and a narrow coolant channel flow areas. Therefore, safety evaluation assuming the blockage of coolant channel due to various reasons is essential. For Monju, although measures to prevent the bowing of fuel

 4. Safety

pins and blockage at the inlet of fuel subassembly were taken, a coolant channel blockage accident was analyzed in which one coolant sub-channel (a coolant channel between three adjacent fuel pins) was completely blocked; and it was confirmed that excessive increase in fuel cladding temperature is unlikely and that the integrity of the adjacent fuel pins is maintained.

In addition, a local accident that may lead to fuel failure was postulated as one of the Item 5 events. It was confirmed that early detection is possible by the failed fuel detection system using the delayed neutron method and a significant core damage does not occur because fuel failure would be only localized.

4.4.3 Core disruptive accident

As for CDAs, in the U.S. experimental reactors (EBR-II, etc.) and Joyo, reactor safety was evaluated against the mechanical effect of the upper limit of energy release calculated by assuming hypothetical prompt supercriticality (recriticality). Since the 1970s, safety analysis technologies had been advanced remarkably in the U.S. and the understanding of physical phenomena was greatly deepened through in-pile and out-of-pile safety experiments. Consequently, it became possible to mechanistically analyze the transient behavior of coolant and fuel pins starting from a normal operation condition, to coolant boiling and fuel melting, and the resultant reactivity changes.

For Monju, SAS3D and SIMMER-II codes were introduced to use the latest analysis method through international cooperation with the U.S. (later, the former was revised to SAS4A, and SIMMER-III/SIMMER-IV codes

were newly developed in Japan on the latter). Furthermore, the knowledge obtained from the CABRI in-pile tests jointly performed with France and Germany were effectively utilized^{4,3)}.

A brief description of the CDA analysis results is given below:

- CDA is an accident that might occur only when reactor scram is assumed to fail during an anticipated operational occurrence. Among the two types of unprotected (with failure to scram) accidents, transient over-power and loss of flow, the latter is shown to be more severe.
- Analyses were performed for an entire sequence from accident initiation to whole core melting. It was shown that prompt supercriticality could occur only when conservative assumptions that would increase positive reactivity effects, such as the limiting of discharge of molten fuel from core, were superimposed. Even in such a limiting case, the integrity of the reactor coolant boundary could not be impaired at the maximum energy release.
- As the result of mechanical energy generation, sodium may be ejected to the upper containment through the shield plug gaps (vessel head). Pressure buildup caused by the resultant sodium fire would not impair the integrity of the CV. Thus, the release of radioactive materials to the environment would be appropriately suppressed.
- Concerning the thermal effect of CDA, molten fuel that continues to generate decay heat would be relocated and solidified within the RV, and could be stably retained and cooled over a long period of time (i.e., so-called “in-vessel retention”).
- Safety research on CDA has continued after the safety review for Monju, and the appropriateness or conservativeness of the early safety evaluation were confirmed. In particular, recent research findings showed that the CDA energetics should be significantly less than those from the initial evaluation^{4,4)}. Table 4-3 shows the results of mechanical energy evaluation by reflecting research findings, including newly developed or improved CDA analysis codes and in-pile safety test data.

Table 4-3 Change in mechanical energy evaluated for CDA

	Joyo MK-III	Monju	Remarks
Thermal power	140 MW	714 MW	
Analyzed event	Hypothetical accident	CDA event	
Maximum energy* (normalized by thermal power)	180 MJ (1.29)	330 MJ (0.46)	Thermodynamic potential
CDA analysis based on new research findings	—	110 MJ (0.15)	Thermodynamic potential
	—	16 MJ (0.022)	Maximum kinetic energy estimated by multi-phase multi-component thermal hydraulic analysis
Tolerance of reactor structure*	200 MJ	500 MJ	Integrity was confirmed by structure response analysis.

* Values described in the Application for Reactor Installation Permit

4.5 Risk Assessment for Monju

The probabilistic risk assessment (PRA) methods developed in the U.S. in the 1970s were applied to Monju. A reliability database for sodium components specific to FRs was developed and the data required for PRA, such as the component failure rate, has been continuously expanded⁴⁻⁵.

In the PRA, potential initiating events are systematically identified first, and then the accident sequences from each initiating event are analyzed by successively quantifying the success/failure response of safety systems and components (equipment responsible for safety functions) to assess the occurrence frequency of core damage (Level 1 PRA). Next, the containment failure frequency and the source terms of radioactive materials are evaluated by analyzing the in-vessel and ex-vessel accident progression for each core damage accident sequence (Level 2 PRA).

- A PRA technological base applicable to FRs was established through implementation of the detailed PRA for Monju.
- For Level 2 PRA that evaluates the core damage progression processes, the latest safety analysis codes and in-pile and out-of-pile test data that were obtained through safety researches and international cooperation were used as much as was practicable.

- It was estimated that the core damage frequency (CDF) and the loss of containment function (including the containment isolation failure) were, respectively, in the orders of 10^{-7} and 10^{-9} per reactor year; and hence the risk level of Monju would be at a sufficiently low level compared with that of LWRs.
- The estimated probability of the occurrence of early and large-scale release of radioactive material that is most notable from the risk perspective was much lower: less than 1/10,000 per core damage.
- The PRA results were effectively used for design improvement of the plant protection system, etc. in the detailed design stage and the preparation of accident management measures after the start of operation⁴⁻⁶.

The above results confirmed that the potential risks of Monju are maintained at an extremely low level, and that the application of PRA methods is extremely useful in evaluating the comprehensive appropriateness of safety design and in examining measures to further improve the safety of equipment and operating procedures. Figure 4-5 shows the effectiveness of measures to prevent core damage evaluated using the PRA method. The CDF was significantly reduced by use of the measures, which were not included in the measures for design basis accidents such as the backup shutdown function and the natural circulation function in the auxiliary cooling system⁴⁻⁷.

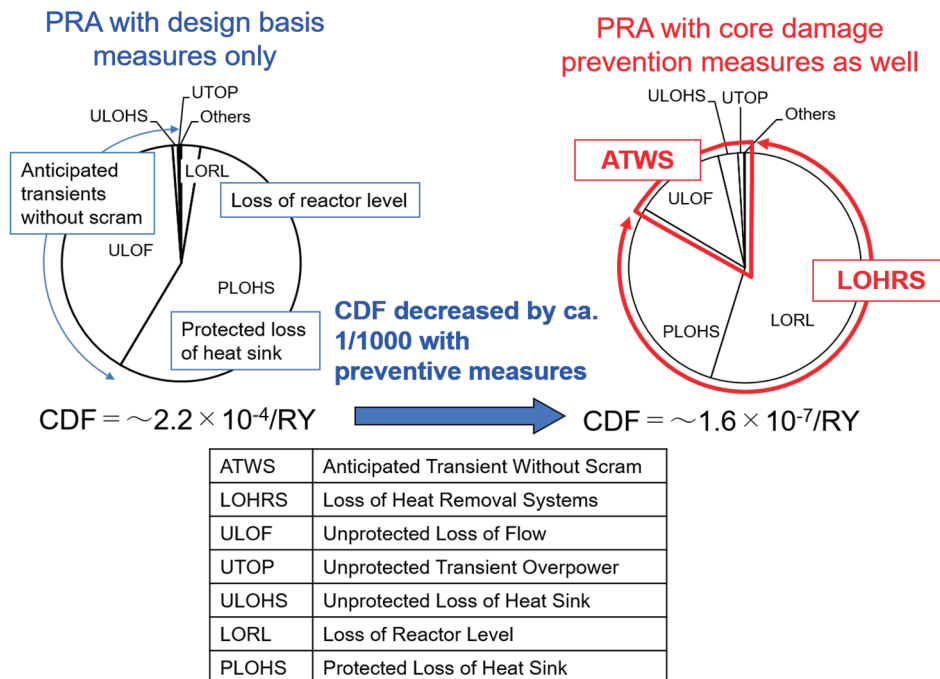


Fig.4-5 Core damage accident sequence groups (Level 1 PRA for internal events)

4. Safety

4.6 R&D for safety design and evaluation

To establish the technological base of safety design and evaluation of Monju, various R&D activities were conducted. Important R&D activities from the perspective of FR safety and their achievements are briefly described below.

4.6.1 Research on fuel failure criterion

Concerning the fuel failure criterion under overpower conditions, comprehensive analysis and evaluation were performed of the in-pile test data obtained from a series of the Transient Overpower (TOP) tests in the Operational Reliability Test program conducted at EBR-II in cooperation with the U.S., and a slow-heating-rate TOP test and other tests of the CABRI in-pile test program that was jointly conducted with France and Germany. As shown in Fig. 4-6, it

was confirmed that Monju fuel with a low density (pellet density of 85%TD, smear density of 80%TD, TD: theoretical density) would not fail even if fuel melt occurs, suggesting a high failure limit, and that the dependence of the failure limit on burnup is minimal within the range of available test data. In addition, the circular marks (o) in the figure represent the data of low density fuels similar to the Monju fuel, and a peak burnup of 10% corresponds to a pellet burnup of 100,000 MWd/t.

Concerning the fuel failure limit during an event that decreases heat removal, “the cladding mid-wall temperature is limited to 830°C or less” (one of the acceptance criteria for “anticipated operational occurrences”) in Monju to prevent a failure of heated fuel cladding due to internal fission gas pressure. This value was set at the lower limit of the database that was available in the initial Monju design phase and taking into account a sufficient safety margin. Thereafter, JAEA also made efforts to expand the database in high neutron fluence range with a focus on slow heating rate conditions by performing out-of-pile rapid heating tests. As a result, it was confirmed that the acceptance criteria used in Monju is sufficiently conservative, as shown in Fig. 4-7. Furthermore, the possibility of discussing the streamlining of the safety margin in the future is suggested.

The R&D achievements concerning in-core local faults include the following, although they are considered supplementary to the safety evaluation of Monju.

- A subchannel analysis code ASFRE that can perform detailed analysis of thermal hydraulics in a fuel subassembly was developed and established as a method to evaluate local planar and porous blockages.
- Various in-pile test results jointly obtained through international cooperation were comprehensively evaluated by including the probabilistic consideration to examine the possibility of the progression from a random fuel failure, via failure propagation, to a whole core involvement. It was confirmed that the consequences of local faults would be covered by those of CDA with a large margin.

4.6.2 Research on sodium leak and fire

When high-temperature sodium leaks in a room of air atmosphere, such as in the Secondary Sodium Leak Accident, sodium reacts (burns) with oxygen and moisture in the air to

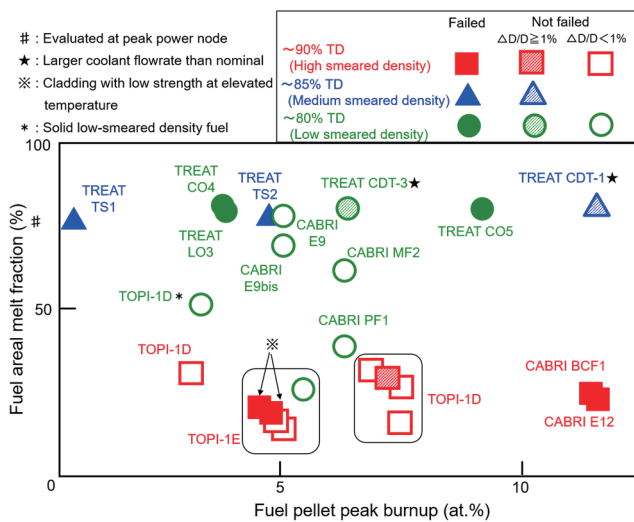


Fig.4-6 Fuel failure/non-failure data obtained from slow overpower in-pile tests for fuel pins of different design and burnup

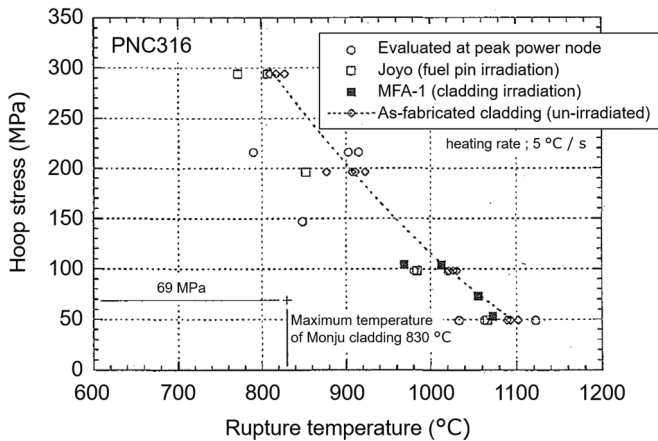


Fig.4-7 Rapid heating rupture strength characteristics of cladding

produce heat resulting from the chemical reaction and smoke (sodium aerosol as a reaction product).

Since the 1970s, experimental studies on sodium fire of various scales and modes (pool fire, spray fire, etc.) were carried out using the sodium fire test facilities. The experimental database was utilized to quantitatively understand the phenomena related to sodium leak and fire, and to reflect the findings to the validation and improvement of safety analysis codes and the design of equipment to mitigate the effects of sodium leak.

A brief description of sodium leak and fire tests is listed in Table 4-4. More than 200 pieces of test data, including small-scale elementary experiments, were accumulated as a database, which was effectively used for the quantitative understanding of sodium fire behavior as well as validation and improvement of the analysis codes. Following the Secondary Sodium Leak Accident, reproduction experiments simulating the structure and scale of the actual plant were conducted to investigate the cause, and the results were used for accident analysis.

For the sodium fire analysis code ASSCOPS, model validation and improvement were performed using the above-mentioned fire test data (Fig. 4-8).

4.6.3 Research on sodium-water reaction

When a tube rupture accident occurs in the SG, high-pressure water leaks into sodium to cause sodium-water reaction that generates heat and pressure, and hydrogen and corrosive reaction products are produced.

Since the 1970s, experimental studies of various scales and conditions were carried out using four types of sodium-water reaction test facilities. The experimental database accumulated was used to quantitatively understand the phenomena associated with sodium-water reactions, reflect the findings to the validation and improvement of safety analysis codes and the design of equipment to cope with sodium-water reaction.

The four types of test facilities and the test programs are shown in Table 4-5. More than 300 tests, including small-scale tests, were performed.

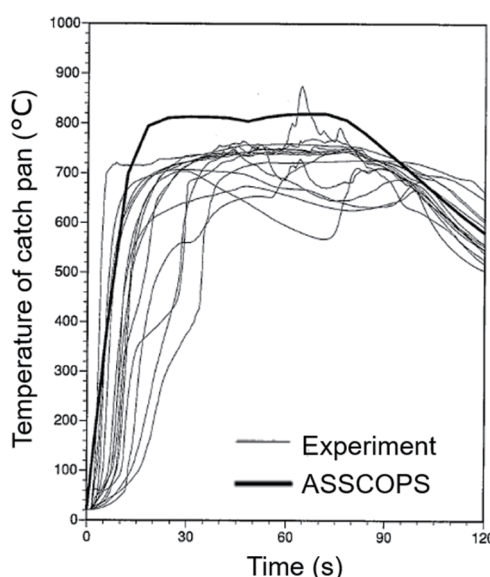


Fig.4-8 Validation of ASSCOPS (Analysis of sodium fire experiments I)

Table 4-4 Overview of sodium leak and fire tests

Period*	Purpose	Main point	Number of tests
In 1995 or before	Pool fire	• Effects of the amount and temperature of sodium, pool area, oxygen concentration, etc.	35
	Spray fire	• Effects of the amount and temperature of sodium, leak rate, oxygen concentration, etc.	51
	Column fire	• Effects of the amount of sodium, leak rate, oxygen concentration, etc. (some tests were common with the pool fire tests.)	22
	Demonstration of equipment to cope with sodium leak	• Specific tests for the liquidity of leaking sodium, and the effectiveness of storage tank on fire suppression • Large-scale integrated simulation test	6
In 1996 or later	Cause investigation of the Monju accident	• Amount of sodium, leak rate, leak height • Accident reproduction experiments (Fire experiments I and II)	4
	Elementary test	• Small-scale pool test • Effects of air flow and moisture • Measures to prevent re-ignition • Clarification of droplet burning mechanism	>100

* Before or after the Secondary Sodium Leak Accident in December 1995

4. Safety

Table 4-5 Overview of sodium-water reaction tests

Device	Main point	Item tested	Number of tests
SWAT-1 (1970)	1/8 the size of Monju evaporator	<ul style="list-style-type: none"> Large leak test Confirmation of pressure relief function Intermediate leak and wastage tests 	27 13 32
SWAT-2 (1972)	Simulation of the entire secondary cooling system of Monju	<ul style="list-style-type: none"> Small leak test + wastage test Development of hydrogen meter Self-wastage test 	160 40 8
SWAT-3 (1975)	Simulation of the whole secondary systems of Monju Reaction container 1/2.5 the size of the evaporator	<ul style="list-style-type: none"> Large leak test Failure propagation test (high-temperature rupture test) 	7 11 (3)
SWAT-4 (1981)	Partial model	<ul style="list-style-type: none"> Minute leak test + self-wastage test 	29



Photo 4-2 Sodium-water reaction test rig (SWAT-3)

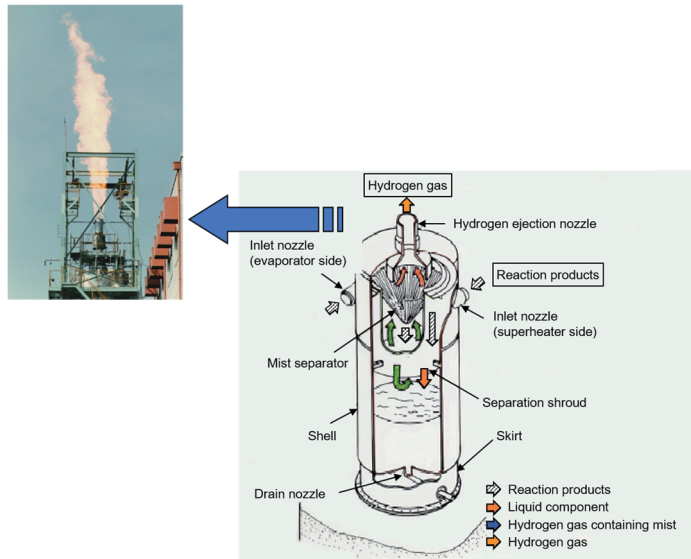


Fig.4-9 Release and burning treatment of hydrogen gas from SWAT-3 test facility

The largest test facility, SWAT-3, is shown in Photo 4-2. Figure 4-9 shows a schematic drawing and a photograph of the release and combustion of hydrogen from the SWAT-3 test facility.

It was confirmed that the wastage on the adjacent tubes by jet impingement of sodium-water reaction products that are generated in the event of a tube rupture is the dominant mechanism of failure propagation, and the relevant phenomena were quantitatively understood through a series of the SWAT tests.

Based on large-scale leak tests, the phenomena related to a short-term initial pressure spike and a long-lasting quasi-stationary pressure, which are important from the perspective of the effects on facility safety, were quantitatively understood, taking into account the large-

est-scale water leak assumed in safety evaluation (design-basis leak equivalent to a failure of 4 heat transfer tubes). In addition, the safety analysis codes were developed and validated. An example of comparison with the test data of the initial pressure spike and quasi-stationary pressure simulated by the SWACS code, which was used for the safety evaluation of Monju, is shown in Fig. 4-10.

4.6.4 Research on core disruptive accident

Among the many research achievements on CDA, those that contributed to advancing accident analysis technology are described below.

JAEA participated in an international joint in-pile test project using the French test reactor CABRI (Photo 4-3). In this program, a total of

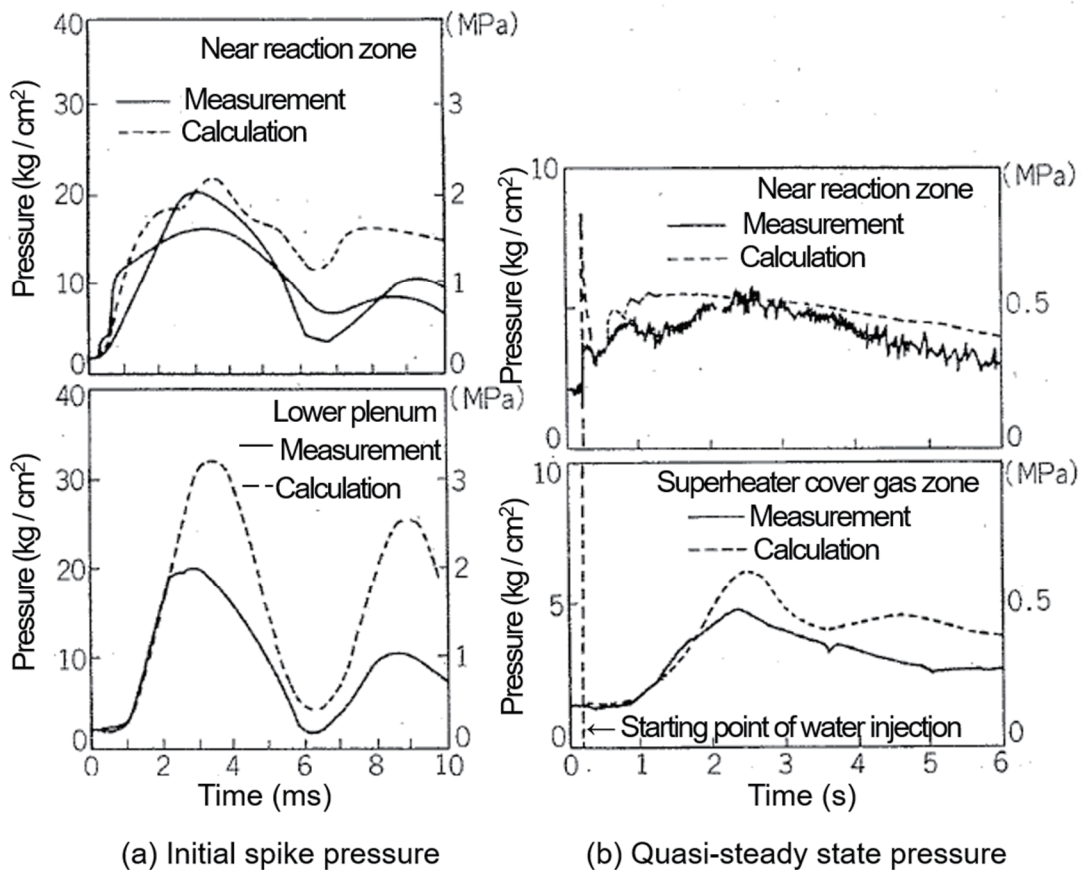


Fig.4-10 Comparison between SWAT-3 tests and SWACS analyses



Photo 4-3 CABRI Reactor Facility
(Courtesy of CEA, France)

63 in-pile tests were conducted, and valuable data were obtained concerning the transient behavior, failure, and post-failure motion of fresh or pre-irradiated FR fuel. In the CABRI tests, accurate test instrumentation using the neutron hodoscope (capable of measuring the change of fuel distribution by selectively measuring the fast neutrons emitted from test fuel) was developed and used.

An example of validation analysis is shown in Fig. 4-11, in which axial relocation behavior of

the molten fuel during the initial phase of CDA was analyzed by SAS4A code and compared with the CABRI test data.

In the process of core damage progression after wrapper tube melting, the method of dealing with the multi-dimensional thermal hydraulics of core materials (fuel, steel, sodium, fission gas, etc.) and the associated space-dependent neutronics becomes prominent. In this field, SIMMER-II, which was introduced from the U.S., was initially used; subsequently, the SIMMER-III (2-dimensional) and SIMMER-IV (3-dimensional) codes were newly developed by JAEA, allowing for a more realistic analysis of the energy release during CDA (Table 4-6).

Concerning the stable cooling and retention of damaged core materials in the RV, experimental research was conducted at the molten core material behavior test facility (Photo 4-4) using various types of simulants. It was confirmed that high-temperature molten material was effectively solidified by the excellent heat transfer characteristics of sodium and relocated in a form (particulate debris bed) that can be readily cooled.

4. Safety

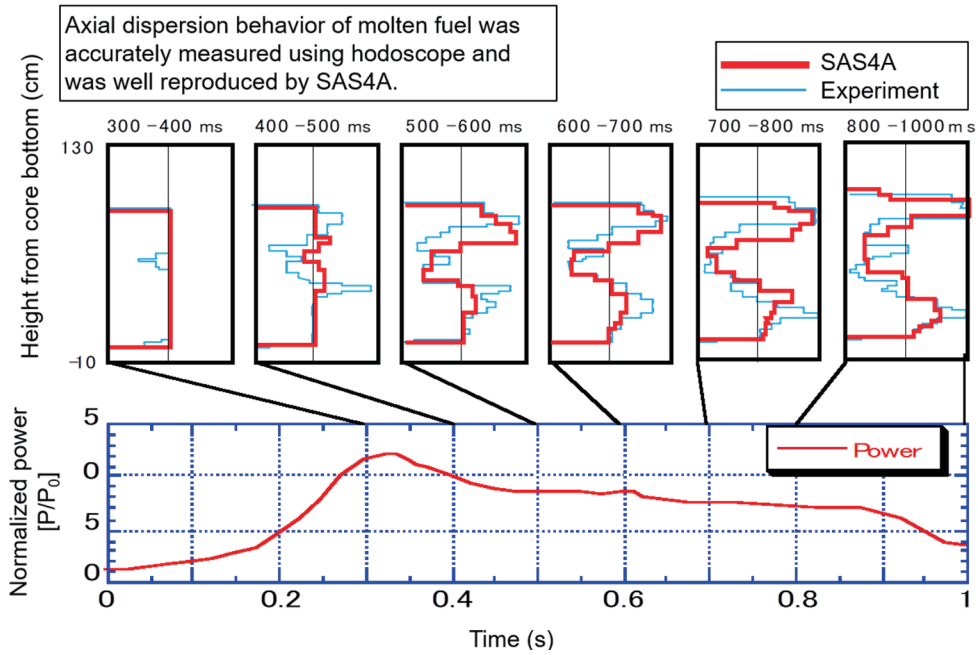


Fig.4-11 SAS4A analysis of fuel motion behavior in CABRI E13 test

Table 4-6 Examples of advanced models of SIMMER-III/-IV

	SIMMER-II	SIMMER-III / -IV
Developer	U.S.: LANL	Japan: JAEA
Dimension	2 (r-z)	2 (r-z) / 3 (x-y-z)
Number of structural components	5	9/15
Number of liquid components	6	7
Number of velocity fields	2	3 or more (maximum of 8)
Phase change	Equilibrium in principle	Non-equilibrium
Equation of state (gas)	Simplified equation (ideal gas)	Solid-critical point (non-ideal gas)
Neutron flux	Diffusion code or TWOTRAN	TWO-/THREE-DANT
Others	—	Increased precision, numerical stability, enhanced V&V

4.6.5 Development of plant dynamics and safety analysis code

A general-purpose, modular-type plant dynamics analysis code, Super-COPD, was developed by incorporating the dynamics analysis code for plant cooling system and the neutronic-thermohydraulic code used for the safety evaluation of Monju with the addition of new models and functions.

The validity and applicability of Super-COPD was confirmed by checking the reproducibility of safety evaluation results described in the Application for Reactor Installation Permit and analyzing the commissioning test data of Monju at powers up to 40%. The natural circulation test performed at Joyo was also analyzed (Fig. 4-12).

Super-COPD can be broadly used not only for plant dynamics analyses in plant design and analyses of anticipated operational occurrences and design basis accidents, but also for broader safety evaluation, such as the assessment of the effectiveness of core damage prevention measures against severe accidents.



Photo 4-4 Molten Core Material Behavior Test Facility (MELT)

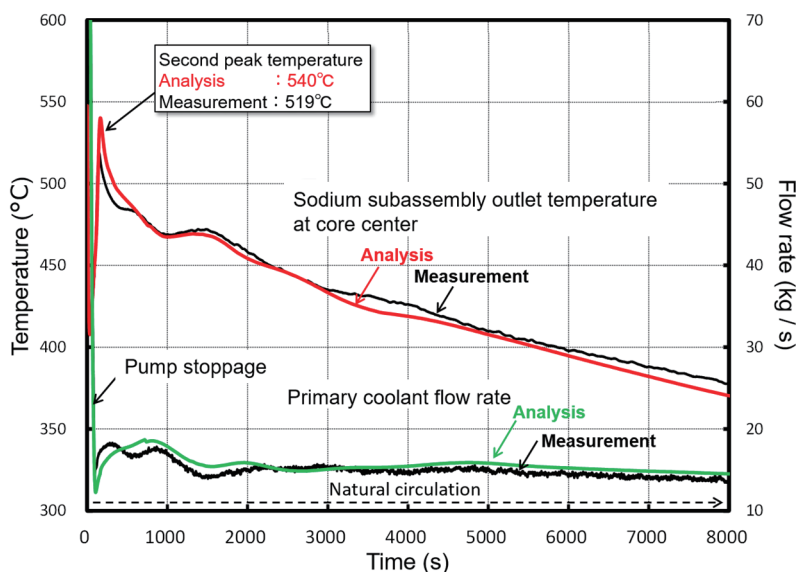


Fig.4-12 Super-COPD analysis of natural circulation experiment in Joyo MK-II core

4.7 Reflection of lessons learned from accidents and failures, and new findings

Continuous efforts were made to confirm and improve the safety of Monju in consideration of the revision of the regulatory acts and standards, and the lessons learned from accidents and failures, as well as new R&D findings.

4.7.1 Improvement of safety following Secondary Coolant Leak Accident

Following the investigation of the cause of the sodium leak from the Monju SHTS piping and the examination of recurrence prevention measures, part of the reactor cooling system was modified to enhance the safety against sodium leak, etc.

- To mitigate the influence of sodium leak in an air atmosphere, the emergency sodium drain time was shortened by modifying the charge and drain system of the auxiliary secondary sodium system. In addition, measures to mitigate the influences of leaking sodium were comprehensively taken for various leak sizes and the effects of chemical reaction.
- On the occasion of modification of the cooling system equipment, the SG tube rupture accident was re-evaluated taking into account the accident in PFR of the U.K., and it was concluded that high-temperature rupture type failure propagation is unlikely to occur in Monju. Nevertheless, in order to further reduce the possibility of this type of failure propagation by early detection of water

leak and rapid blow of water and steam, a pressure gauge was added in the cover gas and the water-steam relief valves were additionally installed in the evaporator inlet and outlet.

4.7.2 Revision of the Regulatory Guide for Reviewing Seismic Design and seismic back-check

The seismic back-check review was performed based on the Regulatory Guide for Reviewing Seismic Design revised in 2006 taking into account new findings from seismology and seismic research. As for Monju, the seismic safety of building/structure and component/piping systems was reevaluated by increasing the design basis earthquake ground motion (horizontal direction) from the original design acceleration of 466 Gal (cm/s^2) to 760 Gal (other simulated seismic waves were also considered). It was confirmed that the acceptance criteria were satisfied and that seismic safety would be ensured⁴⁻⁸⁾.

To ensure an appropriate seismic safety margin, the 100 m-tall stack was reinforced since its seismic margin was reduced for increased design-basis earthquake. The stack strength was increased by installing a damper at the top of the stack to suppress vibration during earthquake and by reducing the number of fixed positions of the support towers. Concerning the seismic stability of the slope on the backside of the plant, a large amount of soil was removed from the slope surface for improved seismic margin.

In addition, as a part of the seismic back-


4. Safety

check, an evaluation of tsunami confirmed that core cooling is still possible by natural circulation heat removal, even if the seawater pump intake limit is exceeded by the postulated tsunami wave.

4.7.3 Safety improvement following the 1F Accident

(1) Safety measures in consideration of the 1F Accident

In consideration of the occurrence of the 1F Accident following the Tohoku Region Pacific Coast Earthquake that occurred on March 11, 2011, and the progress made of the investigation of cause, various safety measures assuming emergency situations, including station blackout (SBO), were immediately taken.

Since most facilities of Monju are placed 21 m or higher above the sea level, they are tolerant against tsunami. However, measures to stop water were taken around the seawater pump at the Monju port and the seawater intake piping penetration.

During SBO, the core cooling by natural circulation of sodium is possible without requiring an electric power source or urgent operator actions such as depressurization of the system and water injection as required in LWRs. The safety on SBO was confirmed through safety evaluation on plant behavior and the improved reliability of valve operations required for switching to a natural circulation heat removal mode.

A summary of the major safety measures immediately taken in Monju is shown in Fig. 4-13.

(2) Safety evaluation of natural circulation cooling

The direct cause of the 1F Accident is the complete loss of all cooling functions caused by SBO and the loss of heat sinks due to the flooding of seawater system equipment and power supply system resulting from a tsunami far beyond the design basis. Postulating a hypothetical large-scale tsunami at the Monju site, the coolability of the core and spent fuel was evaluated.

Concerning the removal of core decay heat, an examination of the conditions required for maintaining natural circulation confirmed that the core can be stably cooled down to a cold shutdown state and the integrity of the coolant boundary is ensured even when taking into account the uncertainties in the cooling capability and the availability of coolant flow paths. As shown in Fig. 4-14, the coolant temperatures

naturally decrease without relying on power supply or operator actions.

Concerning the coolability of the ex-vessel fuel storage tank (EVST), an examination of the conditions required for maintaining natural circulation confirmed that the coolability of spent fuel and the integrity of the EVST are ensured even when taking into account the uncertainties in the cooling capability and the availability of coolant flow paths.

Concerning the spent fuel water pool, an analysis was performed for various conditions affecting the decrease in water level and the increase in water temperature. In the event of SBO, it was confirmed that there would be a large time margin of longer than two months before the top of cans containing spent fuel are exposed to air by water evaporation and that the water temperature would not increase over 70°C.

The validity of the above safety evaluation results was peer-reviewed by an examination committee consisting of outside experts⁴⁻⁹).

(3) Comprehensive safety evaluation

In consideration of the 1F Accident, a comprehensive evaluation of the safety of Monju, a so-called “stress test”, was performed, similarly to the LWR plants in Japan. The events evaluated were earthquake, tsunami, SBO, and the loss of ultimate heat sink. The margin to significant fuel damage was quantitatively evaluated for each of these events⁴⁻¹⁰). As a result, the safety margins for the reactor and EVST were confirmed to be 1.86 and 2.2 times the design basis earthquake, respectively. Against tsunami, it was confirmed that a tsunami reaching the plant installation level, 21 m above sea level, would be tolerable compared with the design tsunami height of 5.2 m. In addition, in case of the SBO and the loss of ultimate heat sink, it was confirmed that continuous cooling would be possible by natural circulation of sodium and natural air ventilation.

Concerning the spent fuel pool, it was confirmed that the margin for earthquakes would be 1.85 times the design basis, and that a tsunami height of up to 21 m would be tolerable. Furthermore, in case of the loss of ultimate heat sink, it was confirmed that cooling would be possible for more than 300 days by supplying water by use of a fire truck.

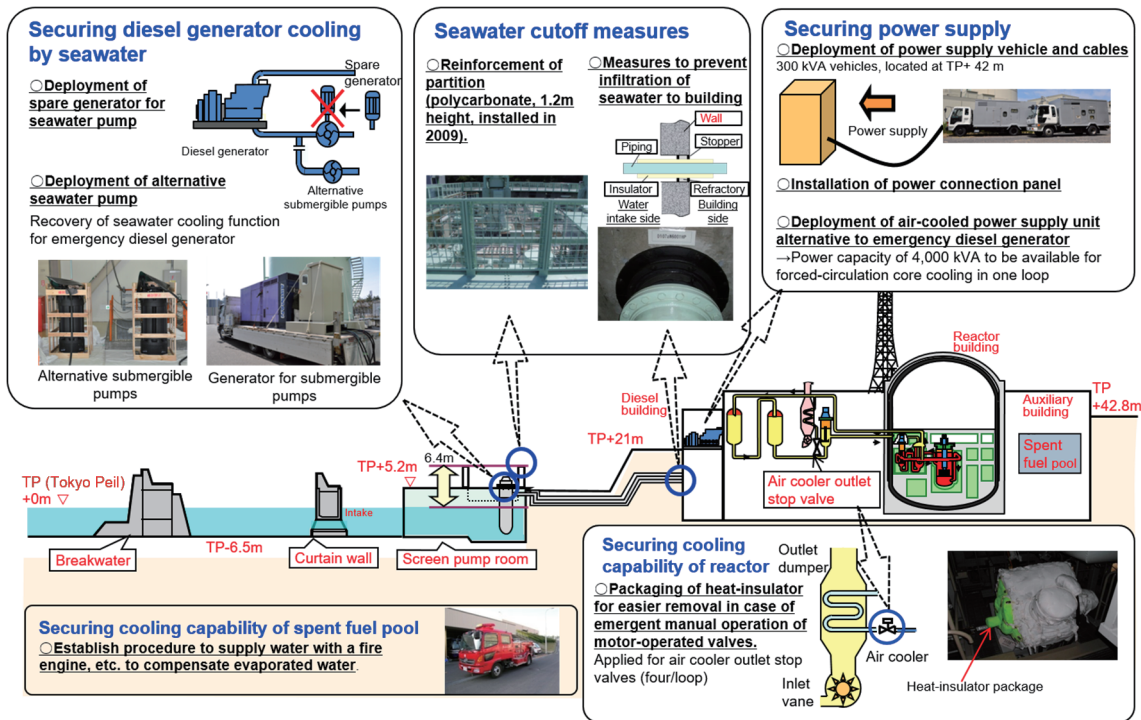
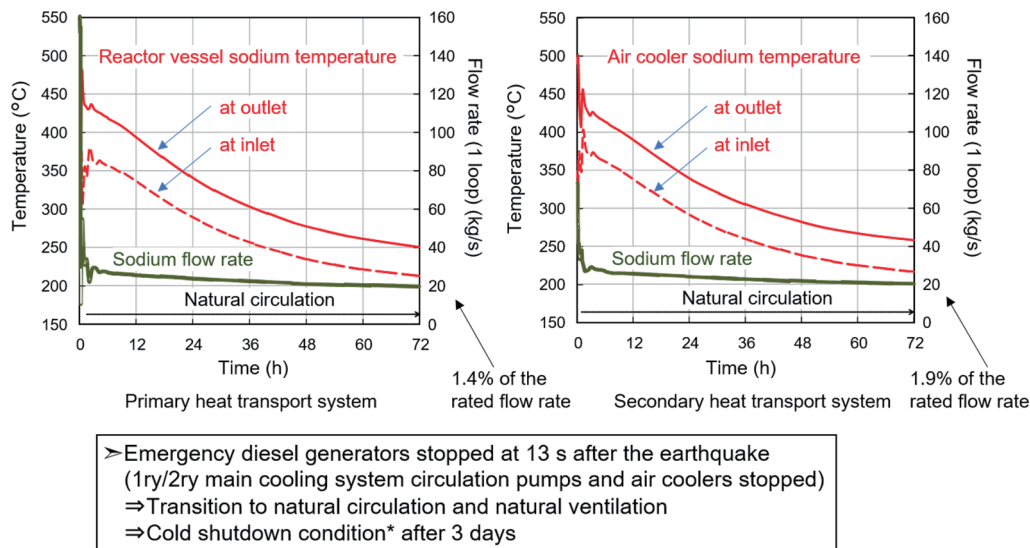


Fig.4-13 Summary of safety countermeasures taking into account the 1F Accident



* All control rods inserted (except for failed rods) and primary coolant temperature stays between 180 and 250°C.

Fig.4-14 Analyses of natural circulation cooling during SBO

(4) Addressing the new regulatory standards

Toward the resumption of operation of Monju after the 1F Accident, JAEA developed a policy to ensure safety with full consideration of safety features of sodium-cooled FRs and based on the trend of international safety standards. This policy was peer-reviewed by domestic and foreign experts⁴⁻⁷. It is particularly important to take into account the characteristics of a low-

pressure system that can virtually eliminate the possibility of containment overpressure failure, different from a high-pressure LWR system, in which containment overpressure failure is a dominant failure mode. It is also important to take advantage of safety characteristics such as retention and cooling of a damaged core inside the RV and the capability of passive decay heat removal by natural circulation.

To undergo a conformity review based on the


4. Safety

New Regulatory Standards enacted in 2013 by the NRA, the prior preparatory effort was made in Monju until the project was terminated at the end of 2016.

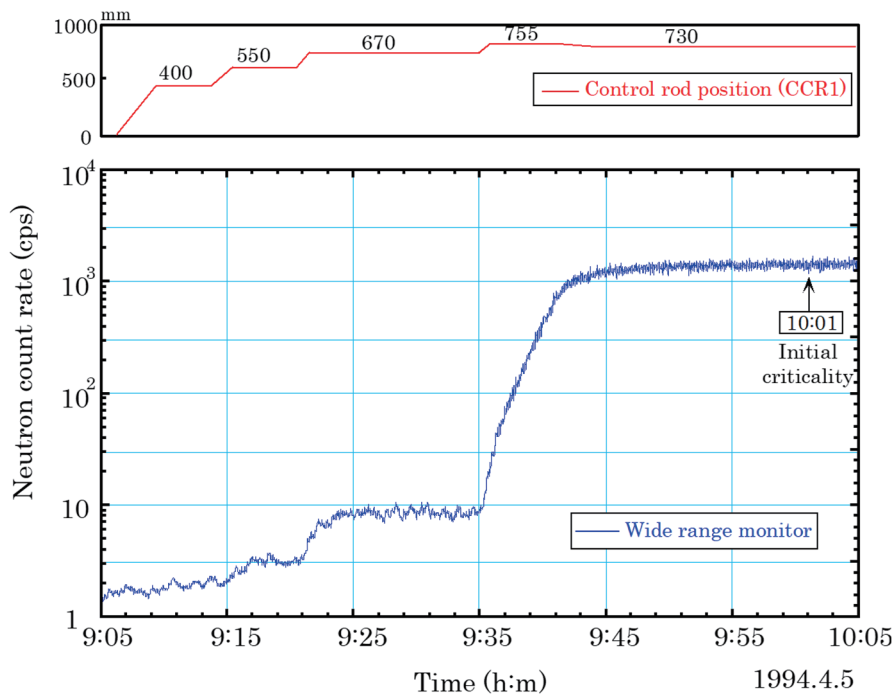
When a new FR development project is studied in Japan in the future, much of the knowledge, including the achievements and

experience in the licensing of Monju, safety analysis codes advanced through applications to Monju, and the supporting experimental database should be applicable.

— References —

- 4-1) Nuclear Safety Commission, Safety Evaluation Policy of Liquid-Metal Fast Breeder Reactors, 1980 (partly revised in 2001) (in Japanese).
- 4-2) JAEA, Annex 8 of the Application for Reactor Installation Permit: Prototype Fast Breeder Reactor Monju, 1980 (amended in 2006) (in Japanese).
- 4-3) Sato, I., Objectives and Main Outcomes of the CABRI In-Pile Experimental Programs for FBR Safety, JNC Technical Review No. 23, JNC-TN1340 2004-001, 2004, pp.1-11 (in Japanese).
- 4-4) Tobita, Y., An Evaluation Study on ULOF Event Sequences in the Prototype FBR; an Evaluation of CDA Reflecting the Latest Knowledge, PNC-TN9410 97-079, 1997, 99p. (in Japanese).
- 4-5) Aizawa, K., Research on Probabilistic Safety Assessment at PNC, PNC Technical Review No. 74, PNC-TN1340 90-002, 1990, pp.43-60 (in Japanese).
- 4-6) JAEA, Report on Development of Accident Management for Prototype Fast Breeder Reactor Installations, 2008 (in Japanese).
- 4-7) JAEA, Safety Requirements Expected to the Prototype Fast Breeder Reactor Monju, JAEA-Evaluation 2014-005, 2014, 275p. (in Japanese).
- 4-8) JAEA, Report on the Result of Seismic Safety Assessment for the Prototype Fast Breeder Reactor Monju following the Revision of the Regulatory Guide for Reviewing Seismic Design of Nuclear Power Reactor Facilities, 2010 (in Japanese).
- 4-9) JAEA, External Evaluation on the Logical Adequacy of the Safety Measures and Coolability of the Reactor Core and Others in Monju considering Earthquake and Tsunami, JAEA-Evaluation 2011-004, 2012, 132p. (in Japanese).
- 4-10) JAEA, Comprehensive Safety Assessments of Monju Taking into Account the Accident at Fukushima Dai-ichi Nuclear Power Station of Tokyo Electric Power Company, JAEA-Research 2013-001, 2013, 392p. (in Japanese).

5. Reactor Physics



- ▶ FR core design methods were established for neutronic, thermal hydraulic, and radiation shielding design through a variety of mockup tests and were applied to the Monju core design.
- ▶ Fuel containing LWR-origin degraded plutonium was designed and fabricated successfully. Change in the plutonium composition during the long-term shutdown was also suitably managed.
- ▶ Core performance was confirmed as designed and physical data applicable to future reactor design were accumulated through commissioning tests up to a 45% reactor thermal power. The performance data of a core containing 1.5% of americium are of great value for future FR design and reactor physics research.

5. Reactor Physics

5.1 Core neutronic design

Monju is a medium-sized core with a volume of 2,000 liters fueled by degraded plutonium. To successfully realize the core, a basic core concept and specifications were selected and reactor physics data were obtained through international cooperation, including mockup critical experiments, to develop the neutronic design method.

5.1.1 Core design overview

The basic policies of the core design include: redundancy of the reactor shutdown systems, shutdown reactivity margin and negative feedback characteristics, power distribution flattening, prevention of power oscillation, and achievement of the high burnup. With these policies, design studies on the basic core configuration, reactivity control, and refueling procedures were performed.

(1) Basic core design

a) Core configuration

The Monju core consists of the core fuel sub-assemblies, the control rod assemblies, the blanket fuel subassemblies, and the neutron shield subassemblies as shown in Fig. 5-1.

The core fuel region consists of inner and outer core regions with different plutonium contents. Core fuel subassemblies with a higher plutonium content are loaded in the outer region to flatten the radial power distribution. The

core fuel pins contain blanket fuel pellets above and below the core fuel pellets. The RB subassemblies are loaded in the surroundings of the core fuel region. With this arrangement, a breeding ratio of 1.2, a design target, is ensured, and neutron leakage from the core is reduced. Outside the blanket regions, the neutron shielding subassemblies are loaded to further reduce neutron leakage.

b) Reactivity control

Reactivity control is exclusively performed by control rods. The control rods are classified into regulating rods and backup shutdown rods. The regulating rods are further classified into coarse and fine control rods, each having both the reactivity control and main shutdown functions.

A helium-bond type control rod element, which contains B₄C pellets in a helium-gas-filled stainless steel cladding tube, is adopted. A cluster of 19 control rod elements are installed in the protection tube that moves up and down in the control rod guide tube (see 7.2.3). Concerning the regulating rods, an anti-vibration structure is adopted to suppress power fluctuation. Namely, six round bumps are circumferentially attached to the lower part of the protection tube, the design of which are based on the result of out-of-pile hydraulic tests.

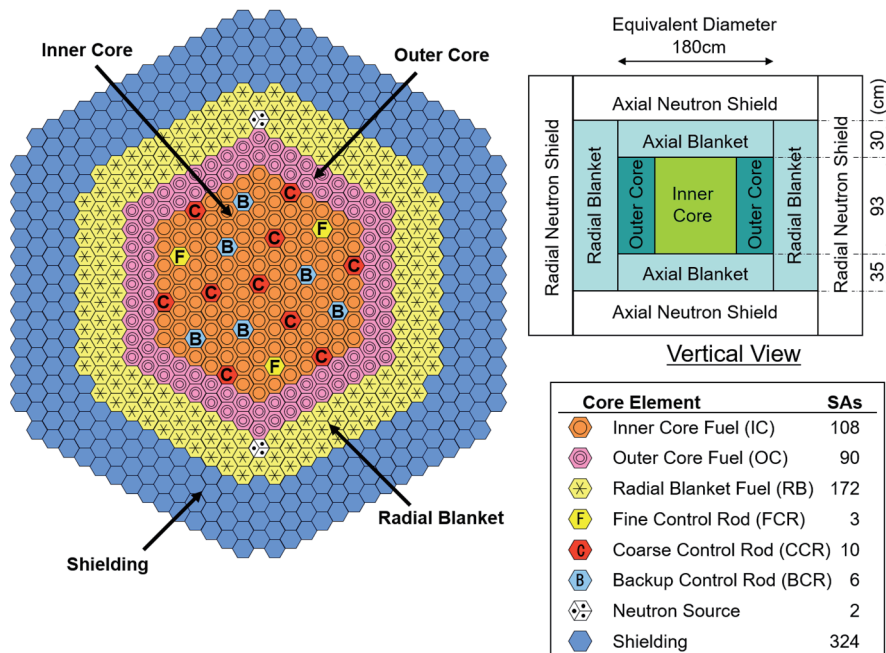


Fig.5-1 Monju core layout

c) Reactivity required for control rods

The regulating rods having a main shutdown function are designed to have a reactivity worth of 7.0 %Δk/k or higher. The required reactivity is broken down into the decrease in reactivity associated with power increase and burnup, the uncertainty in reactivity prediction, the operational margin to ensure a certain differential reactivity in the control rod worth, and the shutdown margin, as shown in Fig. 5-2. The shutdown margin is set at a level 0.4 %Δk/k, which is higher than that for LWRs and is based on the fact that the void reactivity is positive in the core central region of Monju.

d) Low and high-burnup cores

The maximum burnup level of the core fuel is designed to be around 80,000 MWd/t as a core-averaged burnup of discharged subassemblies (high-burnup core). However, it is tentatively set at 55,000 MWd/t (low-burnup core) until the irradiation performance is demonstrated on the anti-swelling properties of SUS316-equivalent stainless steel as shown in Table 5-1.

Table 5-1 Low and high-burnup cores

Items	Low-burnup core	High-burnup core
Burnup of core fuel subassembly (average / maximum) (MWd/t)	55,000 / 64,000	80,000 / 94,000
Operation period (EFPD ^{*1})	123	148
Refueling batch ^{*2}	4-batch	5-batch

*1: EFPD: Effective Full Power Days
 *2: Refueled at dispersed positions

e) Reactivity and power coefficients

Reactivity coefficients are evaluated for Doppler, fuel temperature, structural material temperature, coolant temperature, and core support structure temperature. They are carefully designed to ensure that the power coefficient, an integrated value of the above reactivity coefficients, should be negative.

f) Decay heat evaluation

Since information about the decay heat for plutonium fuel was not available in the early design phase of Monju, an irradiation test was performed at the fast neutron source reactor Yayoi⁵⁻¹. In the test, metal foils consisting of ²³⁵U, ²³⁸U and ²³⁹Pu were irradiated, and gamma and beta rays emitted from the irradiated foils were measured to evaluate the change in decay heat with time. The obtained

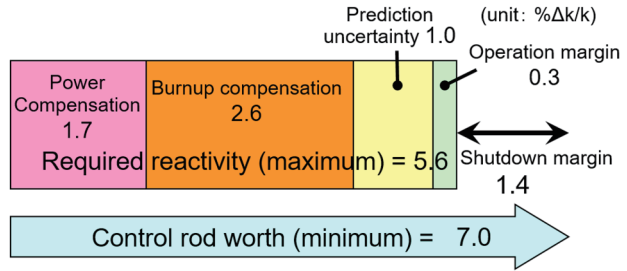


Fig.5-2 Reactivity balance of main shutdown system

data were accurate with a measurement uncertainty of 5%, and were used for the verification of the decay heat design values for Monju and the determination of uncertainty.

(2) Core design with varied Pu composition

a) Use of degraded Pu

The preceding foreign FRs and Joyo mostly use plutonium fuel mainly originating from the reprocessing of gas-cooled reactor fuel or enriched uranium. The plutonium to be used in Monju mainly originates from the reprocessing of LWR spent fuel. The plutonium of LWR origin contains higher-order plutonium isotopes with larger mass numbers (degraded with a smaller fraction of ²³⁹Pu), and thus plutonium compositions may vary clearly according to the timing when Monju is operated. Therefore, the following procedures were adopted to efficiently and reliably cope with a wide variation of plutonium composition:

- An average plutonium composition of LWR spent fuel was used as the reference composition.
- Design calculation was performed based on the reference composition and the core characteristics was reconfirmed when an actual composition becomes available.
- The concept of equivalent fissile content was introduced (see 6.1).
- When the actual excess reactivity is too large, fixed absorber subassemblies are loaded in the radial blanket region to adjust reactivity. On the contrary, when the excess reactivity is too small, operation period is shortened or power is decreased.

b) Countermeasures for long-term shutdown

Monju was forced into long-term shutdown after the Secondary Sodium Leak Accident that occurred during the 40% power test. Because more than 10 years passed since then, the plutonium composition changed by the decay of fissile ²⁴¹Pu (half-life: 14.4 years) to non-fissile

5. Reactor Physics

^{241}Am , significantly decreasing core reactivity. Then it was decided to increase the plutonium content of newly loaded fuel to recover the reactivity loss.

As a result of revised fuel composition, the estimated ranges of the reactivity coefficients changed (Fig. 5-3). For example, the range of revised Doppler coefficient was extended to the less a negative direction. This is due to the shift of neutron spectrum to a higher energy region associated with an increased plutonium content. In the Safety Review of the Reactor Installation Amendment Permit required for the change of fuel composition, the validity of the neutronic design method was confirmed by analysis incorporating the latest knowledge, including the newly developed method of reactor constant adjustment.

5.1.2 Mockup critical experiments⁵⁻²⁾

To optimize the core design of Monju, it was essential to understand and improve the accuracy of nuclear characteristics analysis. Therefore, various critical assembly experiments were performed, a representative of which is the MOZART (Monju ZEBRA Assembly Reactor Test) experiment performed at the critical assembly ZEBRA of the U.K. (Fig. 5-4).

In the MOZART experiment, three types of core configurations that simulated the compositions, dimensions, and control rod insertion conditions were assembled to measure the nuclear characteristics: effective multiplication factor, control rod worth, power distribution, sodium void reactivity, material reactivity worth, etc. The measured values were compared with the calculations using the Monju design method, which were used to determine correction factors and to evaluate uncertainties of the

design method. Subsequently, as a result of comprehensive evaluation, adding data obtained later in the U.S. ZPPR and Japan's FCA, the uncertainties were evaluated to be 0.6% for effective multiplication factor, 5% for control rod reactivity worth, 5% (core region) and 10% (blanket region) for power distribution, 20% for Doppler reactivity, and 30% for sodium void reactivity. These were applied to the core design of Monju.

The MOZART experiment data are registered to the OECD/NEA benchmark data collection⁵⁻³⁾, and used globally for benchmarking analyses.

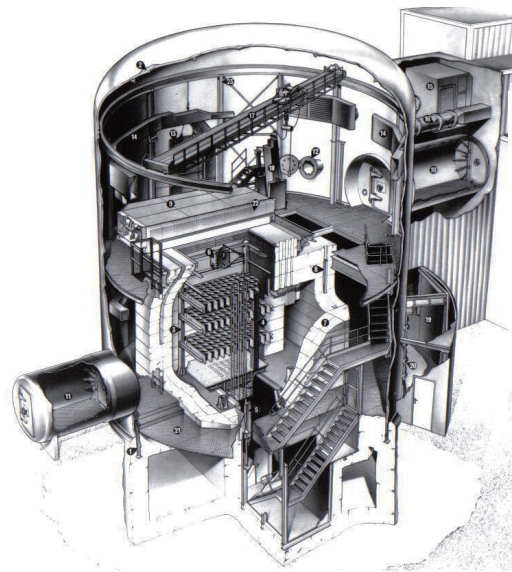


Fig.5-4 ZEBRA critical assembly facility⁵⁻³⁾

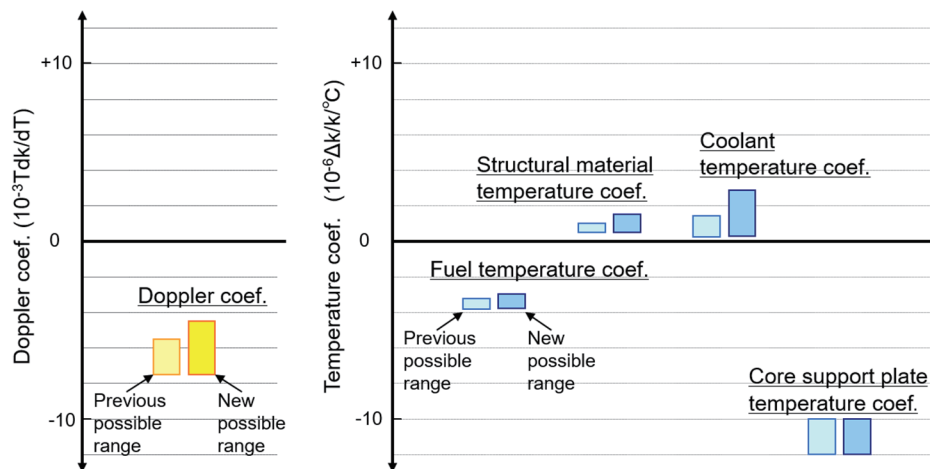


Fig.5-3 Change of reactivity coefficients due to revised plutonium content

5.1.3 Confirmation of nuclear characteristics and data acquisition

Monju achieved initial criticality with 168 core fuel subassemblies in April 1994. Since the analysis accuracy was insufficient in the early development stage, efforts were made to improve accuracy through the MOZART experiment and the development of analysis methods. In the initial criticality approach during commissioning, as much as six fixed absorbers were prepared for cases with excess reactivity much larger than predicted. As a result, the critical mass was as predicted, demonstrating high design accuracy.

In the successively performed reactor physics tests and Core Performance Confirmation Tests, the validity of core design was confirmed and the data on reactor core characteristics were acquired.

In particular, due to the decay of ²⁴¹Pu, the core tested during the SST that was resumed in May 2010 (Core2010) became a globally unprecedented core with an ²⁴¹Am content of about 1.5%, three times larger than that of the core in 1994 (Core1994) (Fig. 5-5). For this reason, valuable data, including the effect of ²⁴¹Am on design accuracy, were obtained through comparison of the data obtained in Core2010 and Core1994.

(1) Neutronic design validation

As for the validity of the neutronic design of Monju, it was demonstrated that the nuclear characteristics data obtained in Monju satisfied

the neutronic limits. The data include excess reactivity, reactivity control characteristics (reactivity control capability, shutdown reactivity margin, and maximum reactivity insertion rate), power coefficient, temperature coefficients, and the maximum linear heat rate based on the measured reaction rate distribution.

a) Excess reactivity and control rod worth

It was confirmed that the excess reactivity (a margin for reactor operation) and the control rod worth (capability for reactor shutdown) both satisfied the neutronic limits, suggesting that the as-designed performance was achieved (Table 5-2).

Table 5-2 Conformance with neutronic limits

Item		Limiting value	Measured value	
			Core1994	Core2010
Excess reactivity (180°C)		0.057 or less	0.031	0.006
Reactivity control effect	Main shutdown system	0.067 or more ^{*1}	0.085	0.074
	Backup shutdown system	0.067 or more	0.074	0.069
Shutdown reactivity margin ^{*2}	Main shutdown system	0.01 or more ^{*2}	0.054	0.067
	Backup shutdown system	Keeping the core subcritical	Good	
Reactivity insertion rate		Main shutdown system 8×10 ⁻⁵ Δk/k/s or less	5×10 ⁻⁵ Δk/k/s	5×10 ⁻⁵ Δk/k/s

*1. In cases where a regulating control rod with the maximum reactivity worth (CCR1) cannot be inserted to the core
 *2. [controlled effect] - [excess reactivity]

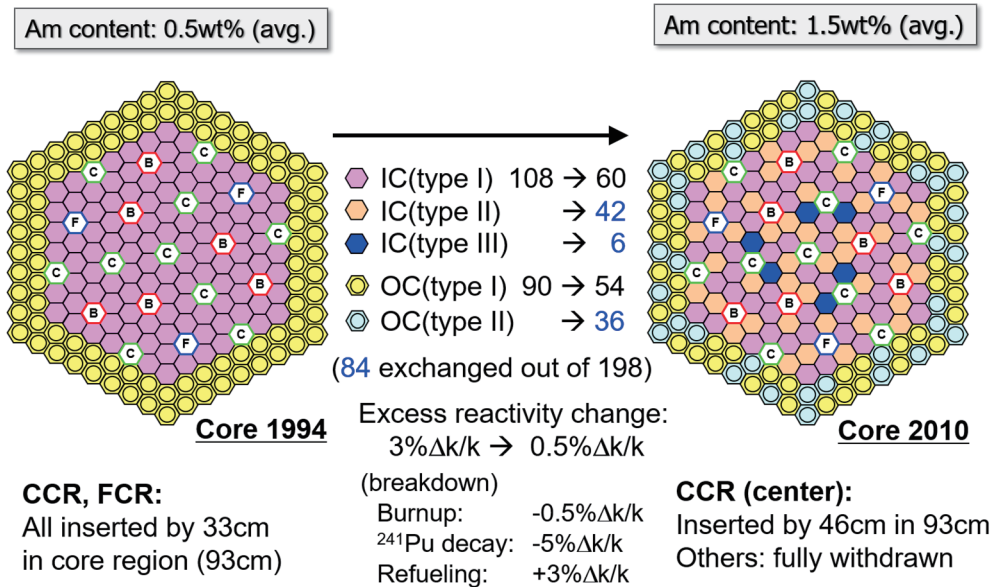


Fig.5-5 Core configurations of Core1994 and Core2010

5. Reactor Physics

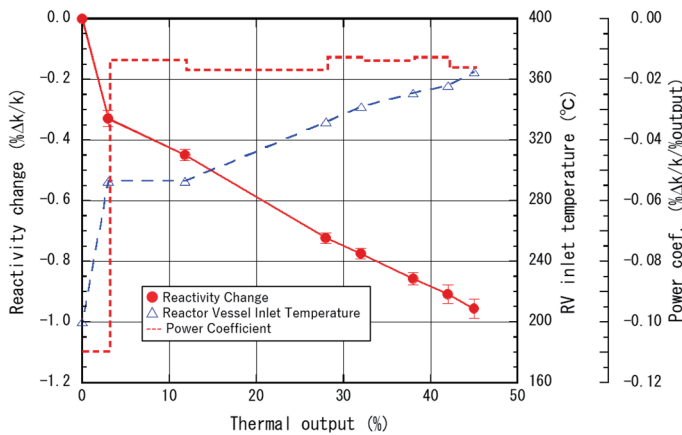


Fig.5-6 Measurement of power coefficient

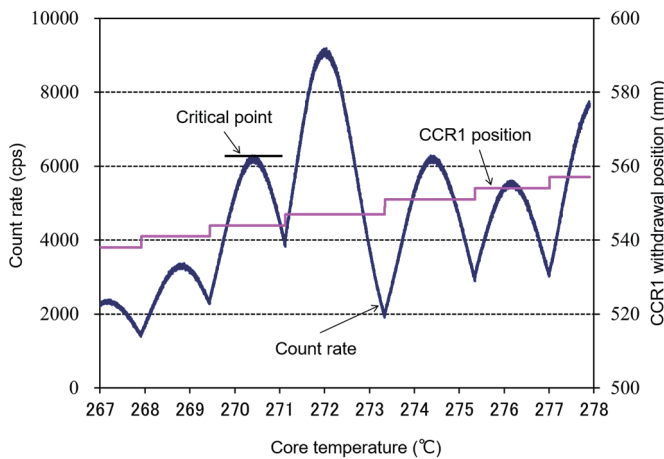


Fig.5-7 Measurement of isothermal temperature coefficient

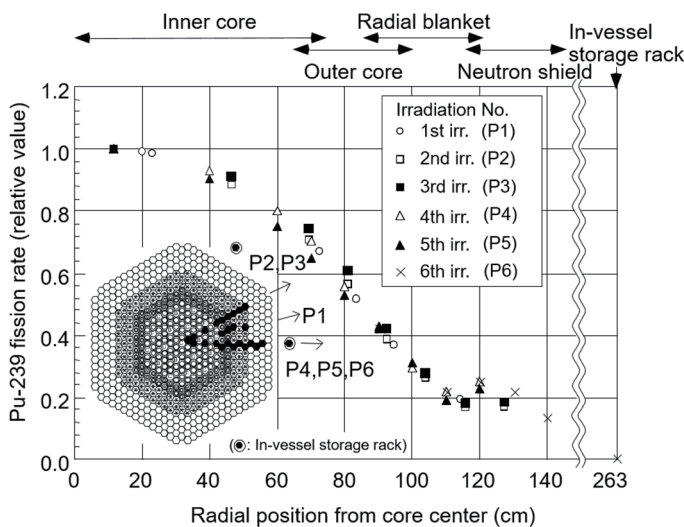


Fig.5-8 Radial distribution of ²³⁹Pu fission rate

b) Power coefficient measurement

Measurement of the reactivity change during the power increase from zero to a thermal power of 45% confirmed that the power coefficient is negative over the entire power range (Fig. 5-6).

c) Isothermal temperature coefficient

The isothermal temperature coefficient is defined as the change in reactivity when the core temperature is uniformly increased. The temperature was gradually increased by heat input from the coolant circulation pumps, and the change in reactivity was measured by the change in control rod positions for the temperature increase from 190°C to 300°C (Fig. 5-7), confirming that the isothermal temperature coefficient was negative.

d) Power (reaction rate) distribution

Using the experimental fuel assemblies incorporating the neutron detection foils, the reaction rates of the foils were measured.

As an example, the radial distribution of ²³⁹Pu fission rate is shown in Fig. 5-8. Also the data concerning ²³⁵U and ²³⁸U fission reactions and ²³⁸U capture reaction were obtained. By correcting the calculated values using the C/E values, it was evaluated that the maximum linear heat rate during rated power operation would be no greater than the design limit of 360 W/cm.

e) Breeding ratio

The breeding ratio was also evaluated similarly using the C/E values, which confirmed that the breeding ratio of 1.2, a design target, would be achieved (Table 5-3).

Table 5-3 Evaluation of breeding ratio based on reaction rate distribution measurement

Core region		Blanket region	
Inner	Outer	Axial	Radial
0.399	0.208	0.217	0.361
0.607		0.578	
1.185			

Note) Calculation corrected by the C/E values of the reaction rate distribution

f) Design method validation

Figure 5-9 compares the measured and analyzed values of the major nuclear characteristics. The measured and analyzed values agreed well within the design margins, confirming the validity of the core design method.

(2) Advancement of analysis methods

After establishment of the design method, analysis methods and the nuclear data have been improved further. For example, concerning analysis codes, it has become possible to accurately model the resonance self-shielding effect of nuclear reaction cross-sections through processing with an ultra-fine energy group structure. In addition, it has become common to take into account the transport effect in a three-dimensional core calculation. The analyses by these newly developed methods were compared with the obtained data.

Figure 5-10 shows the C/E values of the control rod worth obtained in Core1994. The C/E values are almost 1.0 with measurement uncertainties of 2% after correcting for the interference effect, which is the change in worth of a control rod caused by insertion of other control rods⁽⁵⁻⁴⁾.

Figure 5-11 shows the validation of the criticality obtained in Core1994 and Core2010. There is a 0.2% difference in the analyses between the two cores when using the nuclear data library JENDL-3.3. This is mainly due to the difference in the content of ²⁴¹Am. The difference becomes negligible when using the revised library JENDL-4.0, suggesting high analysis accuracy of its ²⁴¹Am nuclear data⁽⁵⁻⁵⁾.

The detailed analysis methods were validated for other major nuclear characteristics measured in Monju, with good agreement within the measurement uncertainties. They included reaction rate distribution (power distribution), temperature coefficients, and power coefficient. It is noteworthy that all results were obtained without use of “correction based on critical experiment data” that was introduced in the original Monju core design.

The measurement of temperature and power coefficients, corresponding to the loss of reactivity associated with the increase in core temperature and power, was performed only at thermal powers up to 45%, and might be insufficient for actual reactor data. However, since analysis accuracy was confirmed to be about 5% for both coefficients^{(5-6), (5-7)}, it is possible to reduce and rationalize the design safety margin ($\pm 30\%$ in the original Monju core design) for the temperature and power coefficients. This is also a significant research achievement to be used in future sophistication of core design.

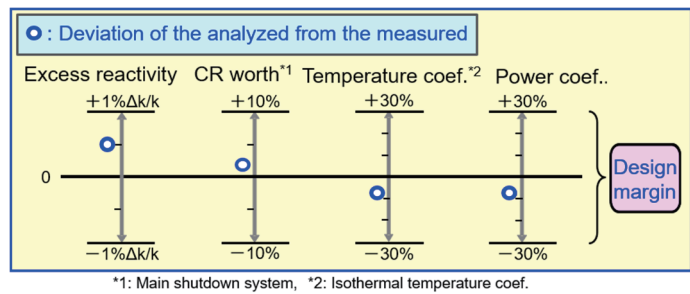


Fig.5-9 Validation of core design margin

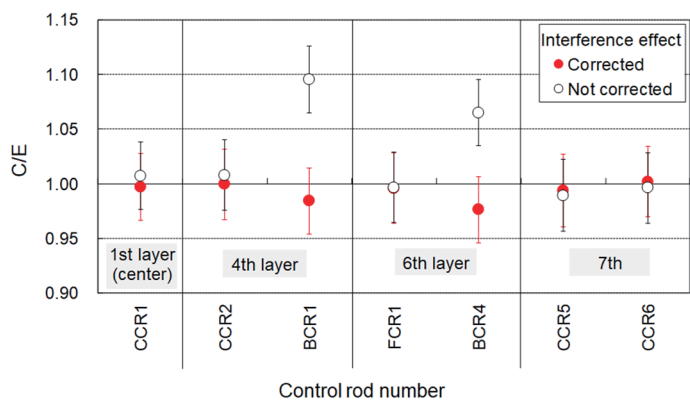


Fig.5-10 C/E values of control rod worth

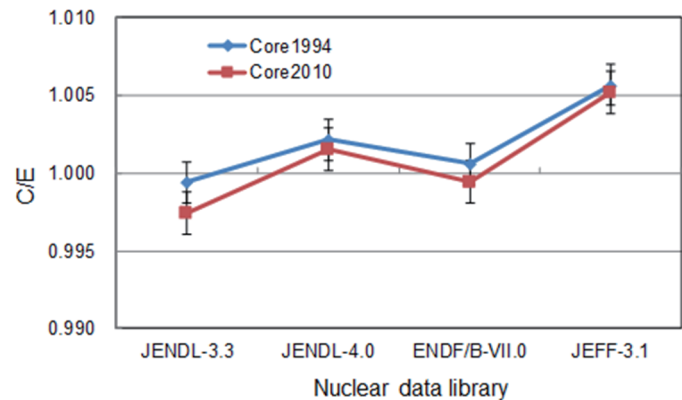


Fig.5-11 C/E values of criticality (k_{eff})

5. Reactor Physics

5.2 Core thermal hydraulic design

In the core thermal hydraulic design, the coolant flow rates to be distributed to various core elements, such as the core and blanket fuel subassemblies, and the control rod subassemblies, were determined based on the power distribution in the core that was evaluated in the neutronic design. The maximum temperatures of coolant, cladding, and fuel were then evaluated. In this process, the design margin based on the hot channel factors was taken into account to conservatively satisfy the thermal design limit.

These are described in the following sections in detail.

Table 5-4 Design values of in-core flow distribution

Zone	Maximum assembly power (MW) (core / core + axial blanket)	Assembly flow rate (kg/s)
1	4.58 / 4.67	21
2	4.34 / 4.43	20
3	4.12 / 4.20	19
4	3.82 / 3.89	17
5	3.65 / 3.71	16
6	4.12 / 4.17	19
7	3.35 / 3.40	16
8	2.96 / 3.00	14
9	0.858 / 0.953	4.6
10	0.384 / 0.432	2.1
11	0.196 / 0.224	1.0

5.2.1 Coolant flow distribution

(1) Characteristics of flow distribution

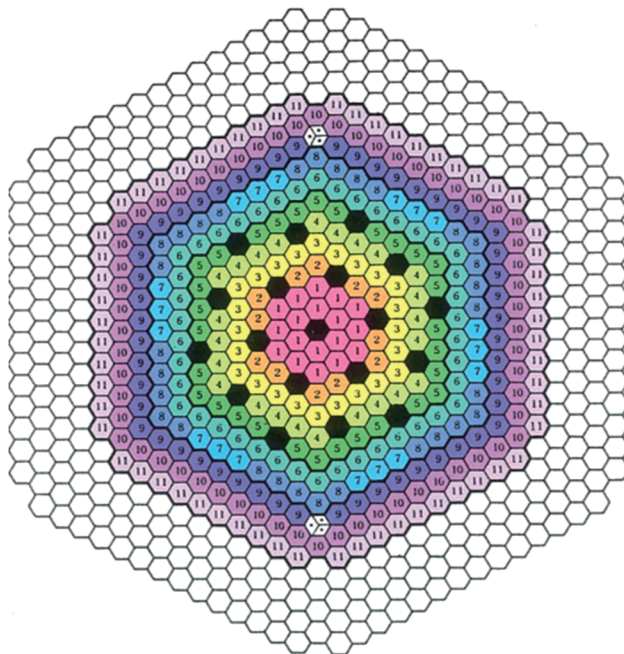
The heat generation density in fuel varies with the fuel composition and location in the core. Then the coolant flow distribution is determined so as to flatten the subassembly outlet temperatures, and thereby to suppress the peak cladding temperature at the rated reactor power.

The core coolant flow is distributed to 11 zones: 8 core fuel zones and 3 blanket fuel zones (Fig. 5-12). The subassembly-wise flow rates and power are listed in Table 5-4.

(2) Confirmation of flow distribution by mockup test

Mockup tests were conducted using a water hydraulic test loop to comprehend the following characteristics and mechanisms that are important to the design of the flow distribution in the RV:

- Pressure drop characteristics of various core elements, including the core fuel subassembly,
- Flow regulation mechanism at the core fuel subassembly inlet, consisting of the entrance nozzle and connecting tube,
- Flow regulation mechanism in the low pressure plenum, and
- Hydraulic characteristics in the low pressure plenum.



Index	Flow rate zone	
1	Zone 1	Inner core
2	Zone 2	
3	Zone 3	
4	Zone 4	
5	Zone 5	
6	Zone 6	Outer core
7	Zone 7	
8	Zone 8	
9	Zone 9	Radial blanket
10	Zone 10	
11	Zone 11	
●	Control rod	
★	Neutron source	
○	Shielding	

Fig.5-12 Flow rate zone allocation in the core

Furthermore, an integral test was performed using a half-scale model in which the above pressure-drop elements were incorporated to confirm the flow conditions and the flow distribution at various parts in the RV. The results of the mockup tests were reflected to the design.

(3) Measurement of core flow distribution

In SST, the core subassembly flow rates were directly measured using a specially prepared flow measurement device to confirm the appropriateness of the core flow distribution.

A comparison between measured and calculated values showed good agreement within 2% (Fig. 5-13), and hence it was directly confirmed that the flow distribution design based on water mockup tests was effective.

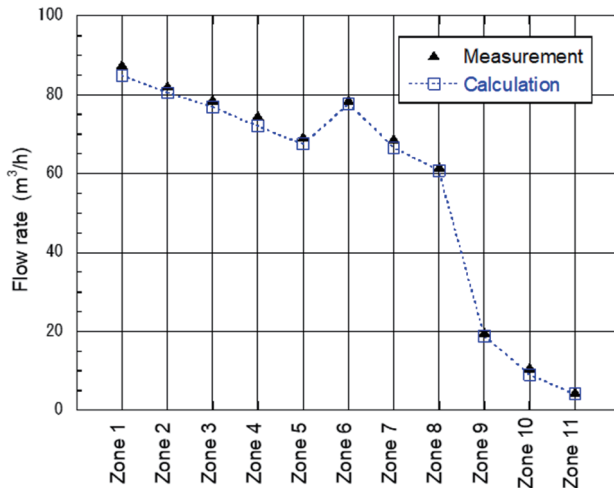


Fig.5-13 Measurement of flow distribution

5.2.2 Maximum temperature evaluation in core fuel subassembly

(1) Temperature evaluation by subchannel analysis

The maximum coolant and cladding temperatures during rated power operation were evaluated by subchannel analysis.

In the subchannel analysis, the interior of a core fuel subassembly is discretized into triangle flow channels (subchannels), each of which is surrounded by 3 fuel elements or by 2 fuel elements and wrapper tube wall (Fig. 5-14). The energy conservation equation is solved for each subchannel by inputting the coolant flow rate and temperature at the subassembly inlet.

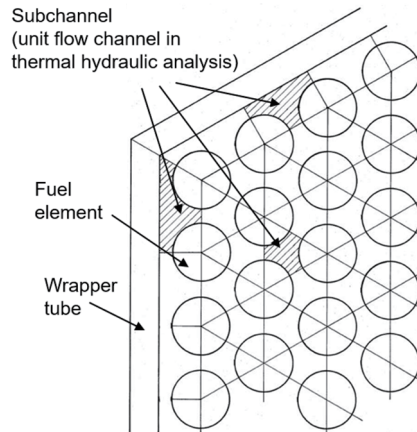


Fig.5-14 Subchannel analysis model for a fuel subassembly

The effects of heat transfer and coolant flow between subchannels (thermal mixing and cross flow) and the difference in flow rates between inner and peripheral regions (peripheral flow effect) were considered based on thermal hydraulic tests with a simulated fuel pin bundle submerged in sodium or water.

(2) Maximum fuel temperature history

Evaluation of the maximum fuel temperature was performed at the rated power and 116% overpower conditions in consideration of the gap conductance (H_g) between cladding and fuel pellets as well as the thermal conductivity and restructuring of fuel pellets.

To evaluate the fuel temperature history, fuel temperature of a core fuel element under the most severe thermal condition was analyzed in consideration of the changes in H_g and power distribution with burnup. An example of the analysis results is shown in Fig. 5-15. It was confirmed that the maximum fuel temperature

is the highest at the beginning of lifetime, and that the fuel centerline temperature remains below the melting point over the operation lifetime even if the decrease in fuel melting point with burnup is taken into account.

(3) Hot channel factor

In the maximum temperature evaluation, various factors were taken into account to provide sufficient design margins (hot channel factors). These include manufacturing tolerances, uncertainties in thermophysical properties, power and flow distributions, and the measurement error of reactor thermal power. The results of mockup tests for nuclear and hydraulic characteristics were reflected to evaluate the uncertainties in power and flow distributions. The resultant hot channel factors for the core fuel subassembly were set at 1.20, 1.26 and 1.25 for fuel, cladding and coolant, respectively.

5. Reactor Physics

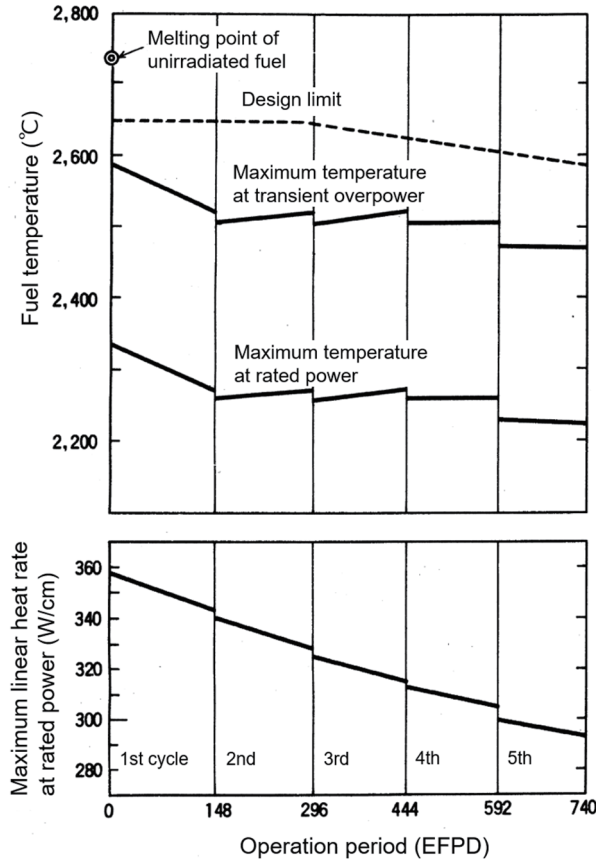


Fig.5-15 Burnup dependence of fuel temperature

(4) Overpower factor

When the reactor power increases excessively during anticipated operational occurrences, the reactor is tripped. The overpower factor, a ratio of the design trip value to the rated power, was set at 1.16 taking into account the margin for operational action, the measurement error of neutron flux level, etc. The maximum fuel and cladding temperatures were designed not to exceed 2,650°C and 830°C, respectively, even taking into account the hot channel and over-power factors.

5.2.3 Measurement of fuel subassembly outlet temperatures

The thermocouples are installed at the outlet of all the core fuel subassemblies and 16 blanket fuel subassemblies.

The temperature changes following a reactor trip from 40% power level are compared between measured and calculated values as shown in Fig. 5-16. The subassembly outlet temperatures in the core (inner and outer) are almost flat. The outlet temperatures in the blanket region are initially about 50°C lower than the core and became slightly higher after the trip. This analysis reproduced the measured characteristics very well⁽⁵⁻⁸⁾.

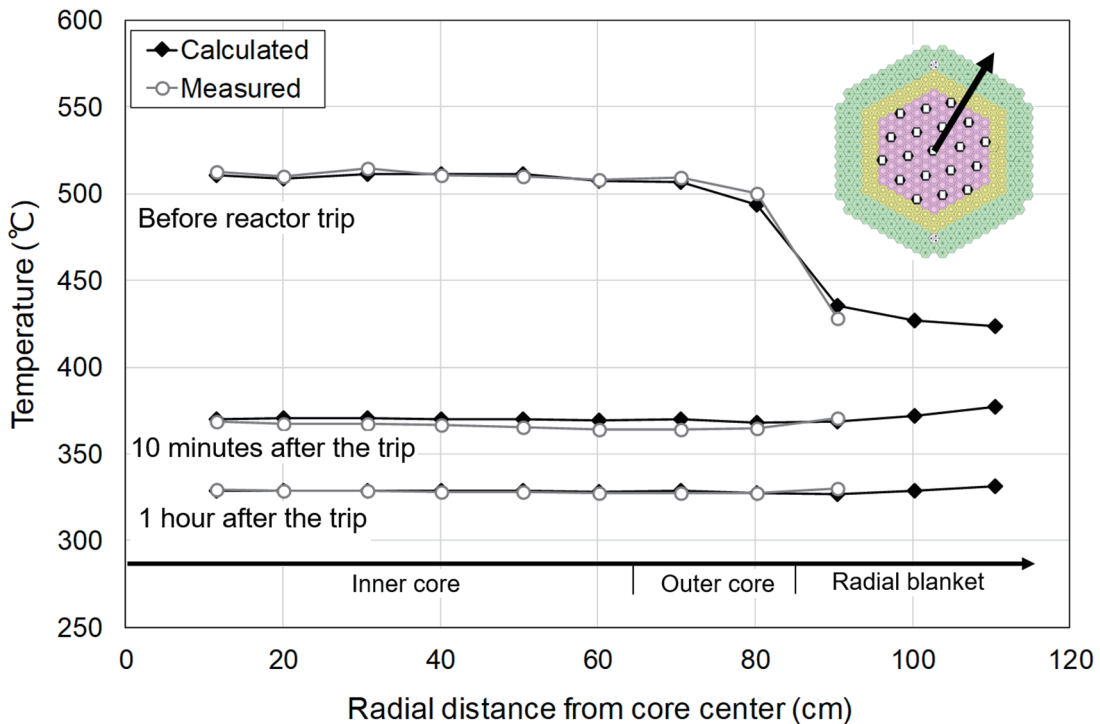


Fig.5-16 Fuel subassembly outlet temperature change after reactor trip at 40% power level

5.3 Radiation shielding design

A shielding analysis system for FRs was developed through the introduction of calculation methods based on the neutron transport theory and their application to the shielding design of Monju. The design was validated using the data obtained during commissioning. Research achievements useful for evaluating rational design margins were obtained.

5.3.1 Development of shielding design method

In the neutron shielding design of the structures surrounding the RV, appropriate measures, including dose reduction in above-core personnel access areas, were taken with consideration of the neutron streaming paths based on the evaluation of neutron flux around neutron instrumentations and neutron fluence for structural material.

Taking into account the fact that the radiation leakage incident aboard the Japanese nuclear-powered ship Mutsu back in 1974 was caused by neutron streaming, a two-dimensional S_n transport calculation code was applied, for the first time in Japan, to the shielding design calculation for Monju. Before its application, valida-

tion of the code and selection of the input parameters, including the energy group set and the number of S_n quadrature, were carried out based on Joyo performance test data, while receiving advice from external experts⁵⁻⁹⁾.

The neutron currents from the core to the shield plug and to the intermediate heat exchanger via the heat transport system piping were calculated and evaluated. Based on the evaluation, measures were taken, including installation of a shielding floor in the reactor cavity, addition of B_4C collars to the primary piping, and enhancement of a stepped structure of the shield plug (Fig. 5-17). These calculations were quite extensive in the days when computer performance was not as advanced.

In the shielding calculation, neutron fluxes must be analyzed with large attenuation of the orders as large as 17 to 18, from the core to above the shield plug. The uncertainty evaluation is another difficulty because the uncertainty associated with calculation modeling depends largely on the shape and material composition of the target. To ensure appropriate design margins, shield penetration testing, survey of the effect of approximation in calculation, etc. were performed. Through these design activities, the shielding calculation method for FRs based on S_n transport calculation codes was established.

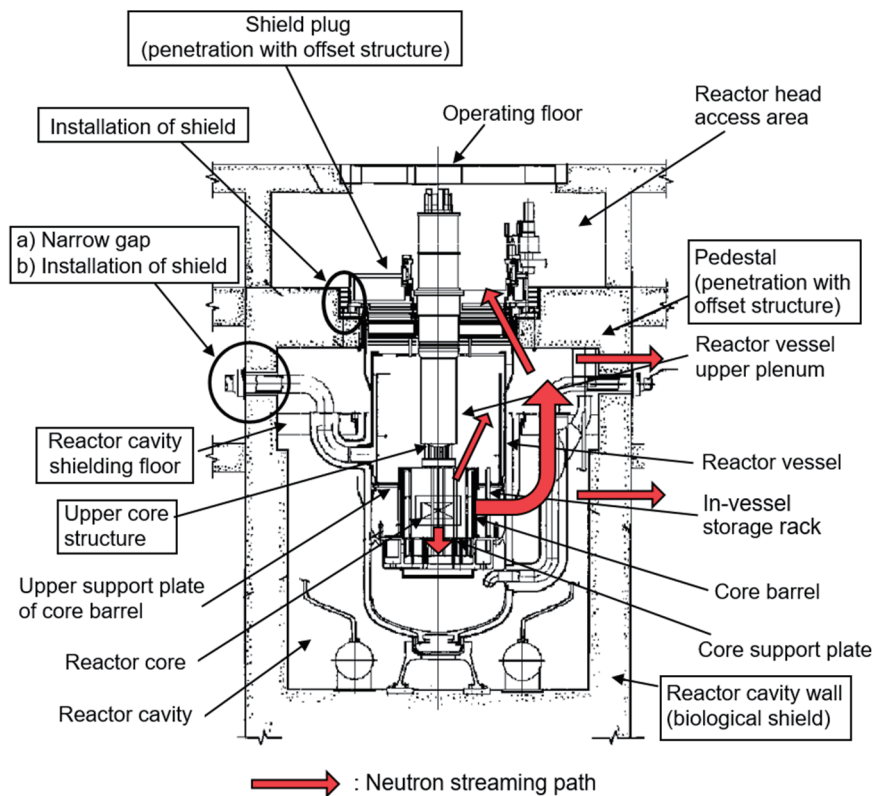


Fig.5-17 Major shielding evaluation points and neutron streaming path

5. Reactor Physics

5.3.2 Design evaluation using SST data⁵⁻¹⁰⁾

Shielding performance in the surroundings of the RV was measured during the reactor physics tests and the 40% power test for design validation and confirmation of the design margin.

The measurements were made using the experimental fuel subassemblies containing the activation foils and the ¹⁰B proportional counter that was inserted into the neutron guide tube located at the reactor upper plenum and

movable up and down therein. The foils were also placed in the pipe shield rooms and PHTS room, and the rem counters in the above-vessel pit room.

As shown in Table 5-5, it was confirmed that the design margins for the RV are appropriate, those for the surroundings of the RV are clearly conservative, and those for the surroundings of shield plug are also clearly conservative, implying further room for rationalization of the margins.

Table 5-5 Evaluation of shielding design margin using measured data

Location evaluated	Attenuation of neutron flux from the core* (order of magnitude)	Calculated/measured	Evaluation of design margin
RV outer surface (at axial core mid-plane)	~7	0.4 to 0.98	Margin (a factor of 3) is appropriate.
Core support plate	~3		Margin (a factor of 2) is appropriate.
Entrance of piping room in RV room / bottom of the gap between pedestal and shield plug	11 to 12	0.4 to 1.3	Margin (a factor of 15 to 20) can be reduced.
Shield plug upper surface	17 to 18	Not detected	Margin (a factor of 2100) can be reduced.

*) Neutron flux attenuation from the core was estimated by the calculated fast neutron flux.

— References —

5-1) Akiyama, M. et al., Measurements of Gamma-Ray Decay Heat of Fission Products for Fast Neutron Fissions of ²³⁵U, ²³⁹Pu and ²³³U, Journal of the Atomic Energy Society of Japan, Vol. 24, No. 9, 1982, pp. 709-722 (in Japanese).

5-2) Zukeran, A. et al., Mockup Critical Experiments for Prototype Fast Breeder Reactor MONJU, Journal of the Atomic Energy Society of Japan, Vol. 18, No. 11, 1976, pp. 672-684 (in Japanese).

5-3) Rowlands, J., The ZEBRA MOZART Programme. Part 1. MZA and MZB ZEBRA Assemblies 11 and 12, International Handbook of Evaluated Reactor Physics Benchmark Experiments, ZEBRA-LMFR-EXP-002, NEA/NSC/DOC (2006)1, OECD/NEA, 2008.

5-4) Takano, K. et al., Control Rod Worth Evaluation for the Monju Restart Core, Nucl. Technol., Vol.179, No.2, 2012, pp.266-285.

5-5) Hazama, T. et al., Criticality Evaluation for the Monju Restart Core, Nucl. Technol., Vol.179, No.2, 2012, pp.250-265.

5-6) Mouri, T. et al., Isothermal Temperature Coefficient Evaluation for the Monju Restart Core, Nucl. Technol., Vol.179, No.2, 2012, pp.286-307.

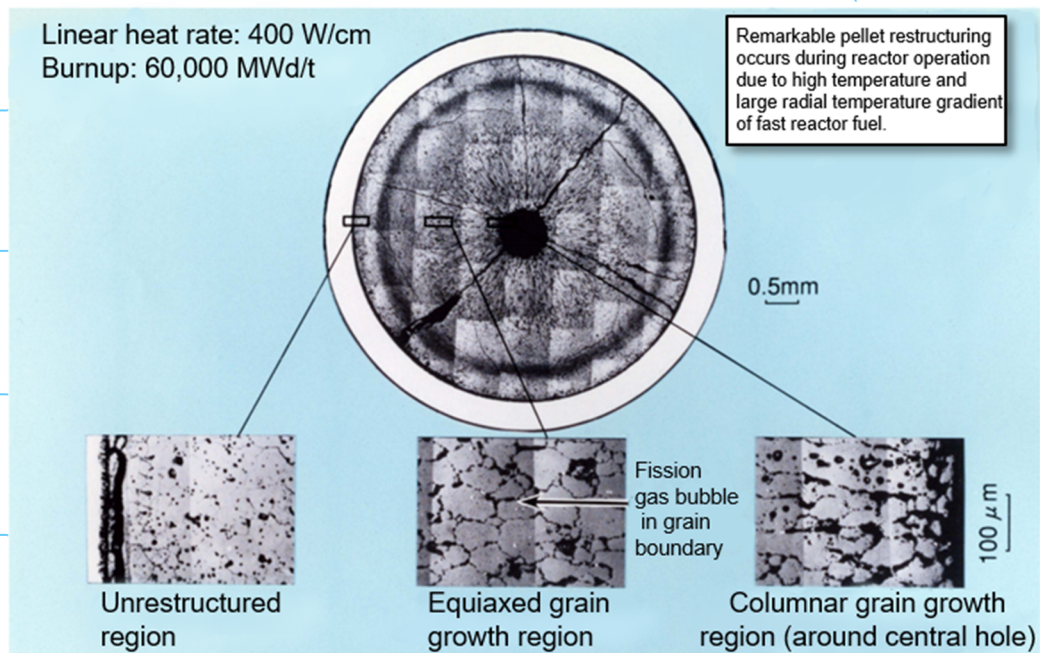
5-7) Taninaka, H. et al., A Refined Analysis on the Power Reactivity Loss Measurement in Monju, Prog. Nucl. Energ., Vol.101, 2017, pp.329-337.

5-8) Mori, T. et al., Validation and Applicability of Reactor Core Modeling in a Plant Dynamics Code during Station Blackout, ICAPP2017, Kyoto, Japan, 2017.

5-9) Special Committee on Fast Reactor Core Design (Shielding Calculation), Shielding Analysis of Joyo Reactor Vessel and Its Surroundings, PNC-TN253 79-02, 1979, 823p. (in Japanese).

5-10) Usami, S. et al., Results of Shielding Characteristics Tests in Monju, JNC Technical Review, No. 11, JNC-TN1340 2001-006, 2001, pp.7-18 (in Japanese).

6. Fuel



《 Typical metallographic observation of irradiated fuel 》

- ▶ The design methods to evaluate fuel temperature and mechanical integrity of FR fuel were developed and improved. The validity of these methods was confirmed through irradiation tests using Joyo and foreign reactors.
- ▶ A wide range of experimental studies were carried out to acquire the physical properties and to understand irradiation behavior of the MOX fuel.
- ▶ Data for the influence of americium content on the fuel thermophysical properties (e.g. melting point and thermal conductivity) were obtained and quantitatively evaluated using newly developed accurate experimental techniques.
- ▶ SUS316-equivalent stainless steel, with superior high-temperature strength and anti-swelling property, was developed as a fuel cladding material of Monju. Data on the material properties were accumulated through various irradiation tests performed domestically and abroad.

6. Fuel

6.1 Characteristics of FR fuel

An important requirement for Monju fuel design is to attain a fuel burnup that is much higher than Joyo. Thus, it is essential that the core material has good resistance to a high fast neutron fluence environment and has high-temperature strength. Also required are the development of technologies for realizing high-burnup fuel and the evaluation of the influence of americium content on the fuel physical properties and the irradiation behavior.

FR fuel generally has the following characteristics compared to LWR fuel as shown in Table 6-1.

- Fuel containing plutonium (major fissile nuclides: ²³⁹Pu and ²⁴¹Pu) is used. The plutonium and fissile plutonium contents are much higher than those of LWR MOX fuel.
- The absorption of thermal neutrons by core material is insignificant in fast neutron spectrum reactors like Monju. Therefore, cladding made of stainless steel can be used instead of Zircaloy cladding used in LWRs.
- Because of the high target burnup, high fuel

temperatures, and a large amount of fission gas generation and release, a large volume of fission gas plenum must be provided inside a fuel pin, a volume sufficient to accommodate fission gas pressure buildup.

- Since fuel pins are densely arranged in the fuel subassembly, wire spacers are used to prevent the pins from coming into contact with one another and to secure space for coolant flow.
- In breeder reactors like Monju, uranium dioxide (UO₂) blanket pellets are installed above and below the core fuel pellets of the fuel element and the radial blanket subassemblies are arranged in the core periphery.

A structural drawing of the core fuel subassembly of Monju is shown in Fig. 6-1. The core fuel subassembly is constituted of 169 core fuel elements, wrapped with wire spacers and arranged in a regular triangular geometry, that are mounted in a regular hexagonal wrapper tube. The wrapper tube is connected with a handling head on the top and an entrance nozzle at the bottom. Each fuel element contains a stack of

Table 6-1 Comparison between FR and LWR fuels

Item	FR (Monju fuel)	PWR (17 by 17 fuel assembly)		BWR (8 by 8 fuel assembly)	
		Uranium fuel	LWR MOX fuel	Uranium fuel	
Fuel specifications	Core fuel material	PuO ₂ -UO ₂	UO ₂	PuO ₂ -UO ₂	UO ₂
	Fissile Pu content (wt%)	16-21	-	8 or less	-
	Pu enrichment (Pu content) (wt%)	32 or less	-	Equivalent to uranium enrichment of 4.1 or less Pellet maximum: 13 or less	-
	²³⁵ U enrichment (wt%)	Depleted uranium	3.4-4.5	0.2-0.4	3.2-3.5
	Pellet outer diameter (mm)	5.4	8.05-8.19	8	10.4
	Pellet density (%TD)	85	95	95	95-97
	Cladding outer diameter (mm)	6.5	9.5	9.5	12.3
	Cladding wall thickness (mm)	0.47	0.57-0.64	0.6	0.86
	Cladding material	SUS316 equivalent stainless steel	Zircaloy-4	Zircaloy-4	Zircaloy-2
	Total subassembly length (mm)	4,200	4,100	4,100	4,470
	Number of fuel rods per subassembly	169	264	264	60
	Fuel rod arrangement	Dense, regular-triangular lattice	Square lattice	Square lattice	Square lattice
	Spacer	Wire	Grid	Grid	Grid
Subassembly outer structure	Wrapper tube	Not applicable	Not applicable	Channel box	
Service conditions	Reactor coolant temperature (°C)	397 (inlet) 529 (outlet)	289 (inlet) 325 (outlet)	288 (inlet) 325 (outlet)	287 (outlet)
	Reactor coolant pressure (kg/cm ² G)	8	157	157	72.1
	Maximum subassembly-averaged burnup (MWd/t)	94,000	55,000	45,000	50,000

MOX fuel pellets (active core fuel) and UO₂ pellets (upper and lower blanket fuel) in a cladding tube.

The isotopic composition of plutonium used for the core fuel changes with a burnup level of spent fuel reprocessed and a cooling period after reprocessing to extract plutonium. In addition, composition change due to the ²⁴¹Pu decay into ²⁴¹Am causes decrease in the fissile worth during the period from fuel fabrication to reactor operation. To cope with these composition changes, the Equivalent Fissile Content Method was introduced when setting the plutonium content in fuel fabrication. In this method, the individual reactivity effects of the isotopes of plutonium, uranium, and americium are converted to the reference reactivity effect of ²³⁹Pu. In the adjustment of fissile plutonium content, the influence of decay of ²⁴¹Pu is also taken into account.

Mechanical loading due to fuel-cladding mechanical interaction (FCMI) is one of the concerns in FR fuel design. In an early Monju design stage, available irradiation data were limited, especially in the high burnup range. Therefore, low pellet density, 85% TD, was conservatively adopted to accommodate fuel swelling due to burnup and, thereby, mitigate the influence of FCMI.

6.2 Fuel design

The Monju fuel was designed following the five design criteria:

- Maximum fuel centerline temperature: Lower than the melting point of MOX fuel
- Cladding strain: Less than 7% increase in the cladding outer diameter
- Creep lifetime: Cumulative damage fraction (CDF) is less than 1, where creep deformation is caused by the tensile stress due to the cladding internal pressure
- Cladding stress: Lower than the design allowable stress in accordance with the ASME standards
- Cumulative fatigue cycle: Less than the design fatigue lifetime, considering the CDF.

In the fuel element design, the fuel design code and cladding stress analysis code were used to evaluate the fuel centerline temperature and the cladding stress, respectively. These codes modeled the fuel thermal conductivity, gap conductance, fission gas release rate, and creep rupture strength, based on experiments.

In the fuel subassembly design, the stress

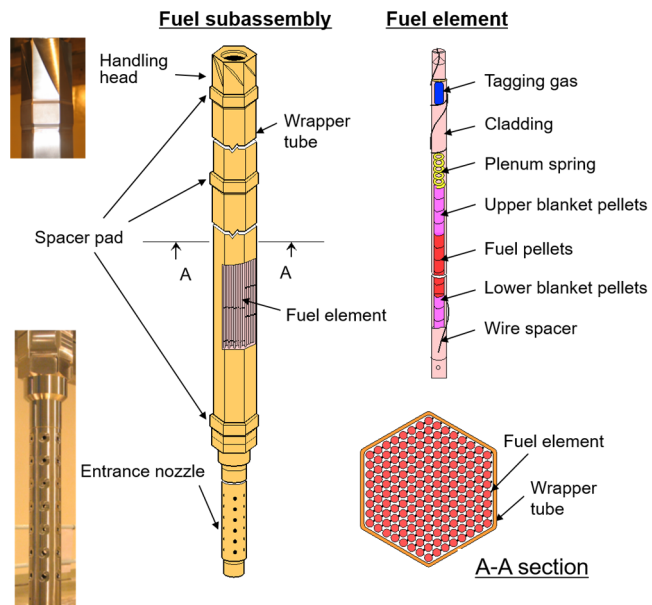


Fig.6-1 Monju fuel subassembly

generated during normal operation and anticipated operational occurrences, and the CDF due to creep fatigue were evaluated. In addition, the integrity of the fuel subassembly was evaluated against the stress generated by a postulated design acceleration of 6 G for fuel transportation and handling.

(1) Maximum fuel centerline temperature

In fuel centerline temperature evaluation, a radial heat conduction calculation is performed based on the heat generated in the fuel pellets, starting from the coolant temperature. The fuel restructuring, which is a characteristic of FR fuel, is taken into account. Because of the high temperatures and steep radial temperature gradient in the fuel, noticeable fuel pellet restructuring (equiaxed grain growth, columnar grain growth, and central hole formation) occurs through evaporation and condensation of fuel material in the voids inside the fuel pellets. A restructuring behavior is schematically depicted in Fig. 6-2, and a typical metallographic observation of test fuel irradiated in Joyo is shown in Fig. 6-3. Fuel restructuring has the important effect of lowering the fuel centerline temperature owing to the formation of a central hole and the increased thermal conductivity of fuel due to fuel densification in the restructured regions. This effect was incorporated in the fuel design and the reactor startup procedure. Namely, in the startup procedure after new fuel loading, the reactor power is increased slowly such that sufficient fuel restructuring takes

6. Fuel

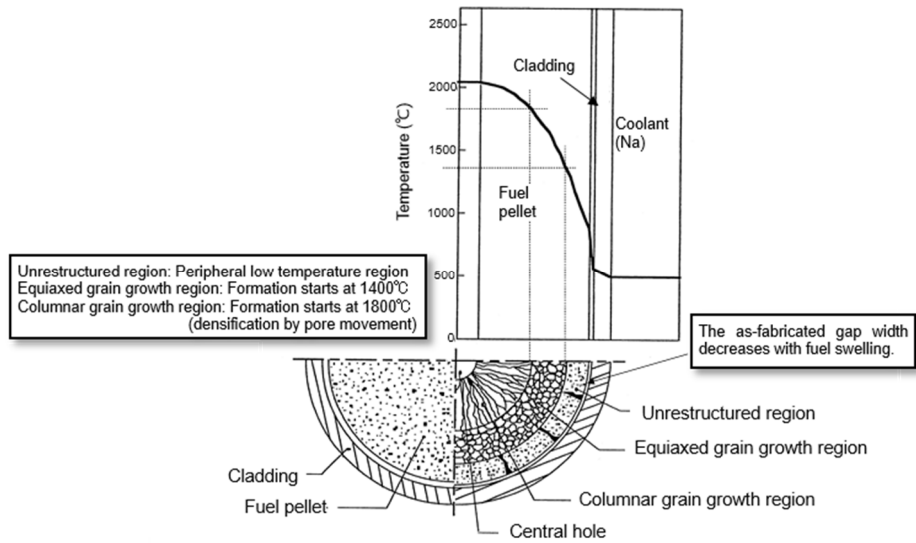


Fig.6-2 Fuel temperature and metallographic change

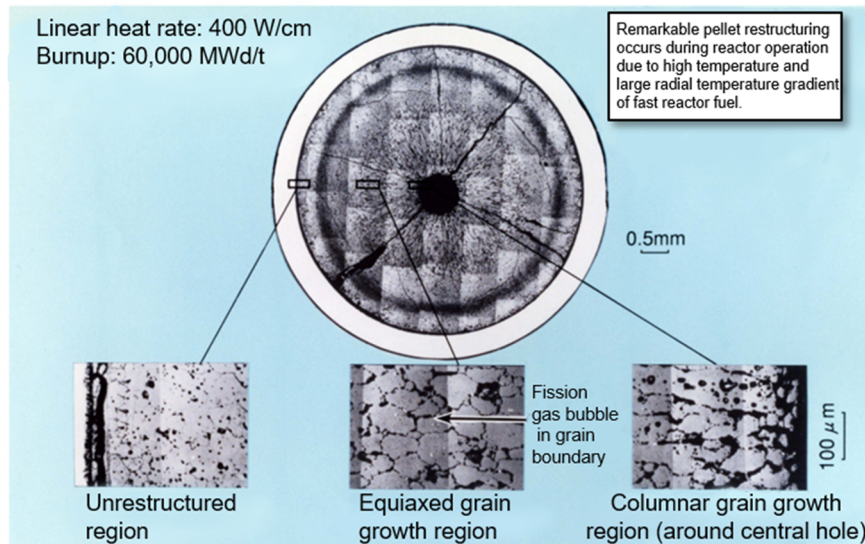


Fig.6-3 Typical metallographic observation of fuel irradiated in Joyo

place. The appropriate setting of the plant protection system is also included in the startup procedure to prevent fuel melting even in the event of anomalies, such as inadvertent control rod withdrawal.

The gap between the fuel pellets and the cladding is filled with helium gas in fuel fabrication and fission gas generated and released during burnup. Appropriately evaluating the heat transfer performance (i.e., gap conductance) is also an important task. In the initial design, the evaluation was based on a power-to-melt (PTM) test performed at EBR-II in the U.S. Later, a PTM test (B5D) and instrumented fuel element irradiation tests (INTA-1 and INTA-2) using thermocouples were performed at Joyo.

The gap conductance was reevaluated based on these test results, and the value used in evaluating the maximum fuel temperature in the initial design was confirmed to be sufficiently conservative.

Figures 6-4 and 6-5 show the results of fuel pellet restructuring and fuel temperature evaluation by the fuel design code SIMPLE, developed for Monju. In the fuel design, the safety margins were appropriately and conservatively considered in the reference calculations, taking into account the uncertainties in power and coolant flow rate as well as the fabrication tolerance of fuel pellets.

In addition, at the time of restart after the Secondary Sodium Leak Accident, the americium

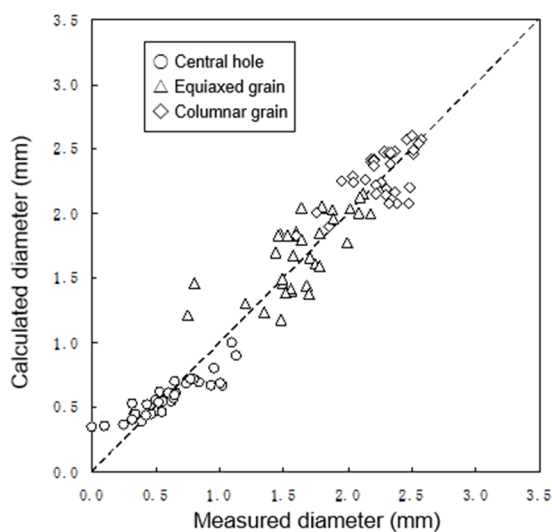


Fig.6-4 Analysis of fuel pellet restructuring by SIMPLE code

accumulation during the shutdown period was an issue for further consideration. It was confirmed that fuel melting could be prevented even if the influence of large americium content up to 2 wt% is assumed on the melting point and thermal conductivity of fuel. The validity of the SIMPLE code was confirmed by a comparative evaluation against a detailed fuel behavior analysis code that was developed later by modeling irradiation behaviors.

(2) Mechanical integrity

The design method to evaluate the mechanical integrity of FR fuel was established through the Monju fuel design.

More fission gas is released from FR fuel than LWR fuel due to higher fuel temperatures and burnup. The resultant high internal pressure, combined with a low external pressure, may cause such problems as larger tensile stress applied to the cladding, and creep deformation and rupture. Furthermore, the fast neutron fluence is higher than that of LWRs by an order of magnitude, and this causes significant swelling of the cladding (i.e., swelling as a result of lattice defects caused by neutron irradiation). Excessive deformation caused by these effects must be also suppressed.

In the mechanical integrity evaluation of Monju fuel, cladding stresses generated by various factors were taken into account with reference to the ASME standards, etc. In particular, the concept of CDF was adopted to prevent creep failure. For the creep rupture strength, which is important for CDF evaluation, various creep rupture test data were used, such as those measured in out-of-pile tests and those

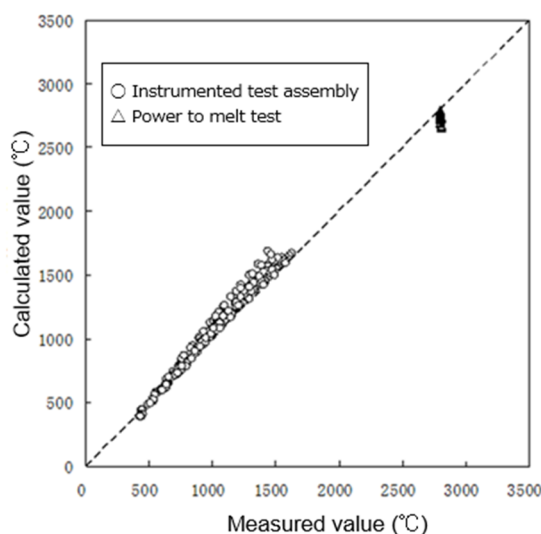


Fig.6-5 Analysis of fuel centerline temperature by SIMPLE code

measured in in-pile tests under sodium environment and fast neutron fluence performed at Joyo.

(3) Irradiation tests for Monju fuel

A variety of irradiation tests were conducted to understand the irradiation behavior and to confirm the integrity of the FR fuel. Initially, irradiation tests were conducted at foreign reactors, including the DFR in the U.K. and Rapsodie in France. After the commissioning of the Joyo MK-II core, irradiation tests were performed primarily at Joyo. In addition, the data from the Transient Overpower (TOP) tests obtained through the U.S.-Japan Operational Reliability Testing (ORT) program at EBR-II were used in the evaluation in the Safety Review for the restart after the Secondary Sodium Leak Accident.

Important achievements of the irradiation tests related to the Monju fuel design are described below:

a) Performance confirmation test of Monju standard core fuel (C3M)

The C3M test is a bundle irradiation test using the fuel elements having almost the same specifications as Monju. Its primary objective was to demonstrate the validity of fuel design and fabrication by setting the maximum linear power and hot spot temperatures as those used in the Monju core design. The pellet peak burnup reached a level equivalent to the design maximum burnup of 130 GWd/t. In the post-irradiation examination (PIE), metallography tests, outer diameter measurement, temperature-transient-to-burst tests, etc., were per-

6. Fuel

formed. Through these tests, the overall integrity of the Monju fuel up to high burnup was confirmed, and the data on important irradiation behavior were obtained.

b) PTM tests (B5D-1, -2)⁶⁻¹⁾

B5D is a series of PTM tests to confirm the margin to the melting temperature of FR MOX fuel and to improve the accuracy of fuel temperature evaluation. To confirm the influence of fuel specifications on the PTM linear heat rate, irradiation tests were performed for various fuel parameters, including fuel pellet density, oxygen to metal ratio (O/M ratio), fuel pellet-cladding gap width, and the presence or absence of tagging gas. In the B5D-1 and B5D-2 tests, high linear heat rate conditions were maintained for 10 minutes, resulting in fuel melting in 3 out of 4 test fuel elements in B5D-1 and all 24 test fuel elements in B5D-2. From the PIE, the maximum fuel melt fraction and the maximum linear heat rate were evaluated to be about 11% and 670 W/cm, respectively. The PTM data obtained from these tests were used in the Safety Review before the restart of Monju after the Secondary Sodium Leak Accident.

c) Tests using Instrumented Test Assembly (INTA-1)

A schematic diagram of the Instrumented Test Assembly is shown in Fig. 6-6. The purpose of the INTA-1 test was to demonstrate the applicability of sensors under in-reactor irradiation and measure a fuel temperature evolution of the Monju fuel. The obtained data were used to validate the fuel design method and improve the fuel behavior analysis code. The INTA-2 test was performed using a large-diameter (outer diameter: 7.5 mm) cladding to obtain the basic data for future large-reactor fuel design. The fuel temperature data directly measured in both the tests were used to evaluate the gap conductance in fuel design along with the PTM data for B5D described above.

d) EBR-II ORT program^{6-2), 6-3)}

The ORT program consists of TOP tests, run-beyond-cladding-breach tests and steady-state irradiation tests. The program was divided into Phase-I (1981-1988) primarily for Monju and Phase-II (1987-1995) for future large-reactor fuel. In a slow-ramp TOP test (TOP1 test), fuel integrity was maintained at a transient over-power up to 90% or higher (peak linear heat rate: 770 W/cm) for fuel elements having the Monju specifications. In a repeated TOP test (TOP-4 test), it was demonstrated that the influence of cyclic overpower on fuel integrity is insignificant.

As described above in a) to d), the various irradiation tests performed at Joyo and foreign reactors demonstrated the validity of Monju fuel design and fuel integrity, and helped establish the basis for future FR fuel development.

Unfortunately, expected high burnup irradiation data had not been obtained in Monju, because full power operation of the reactor plant was not conducted.

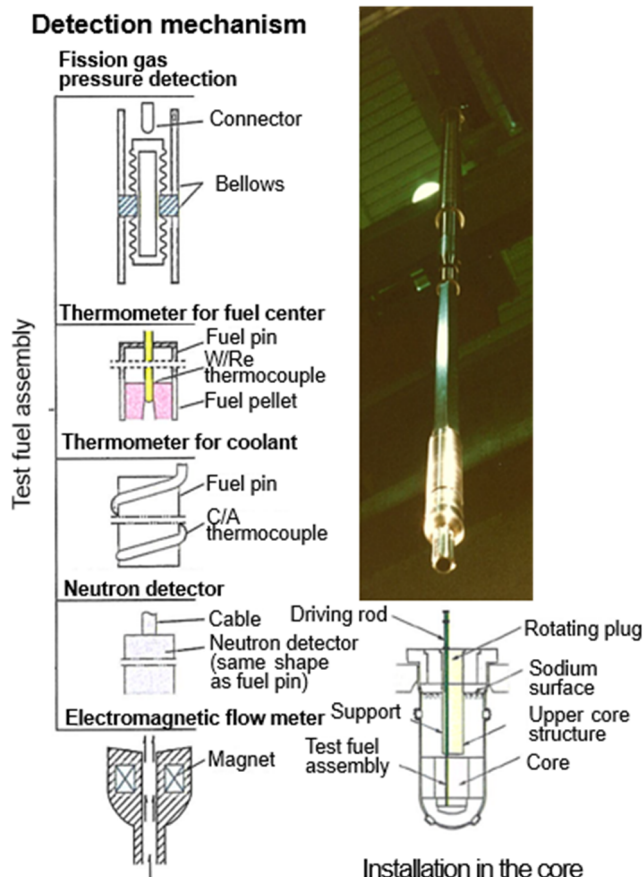


Fig.6-6 Instrumented Test Assembly

6.3 Research on the physical properties of MOX fuel

Early research on the physical properties of MOX fuel in Japan included: development of MOX fuel phase diagrams and acquisition of basic physical properties, such as O/M ratio, X-ray diffraction, metallographic observation, as well as thermophysical properties on the melting point, thermal diffusivity, and thermal expansion coefficient. Subsequently, research was performed on the measurement of physical properties of MOX fuel during irradiation and detailed analyses of irradiation behaviors. Through this research, a wide range of physical

property data on FR fuel were obtained domestically and from abroad. A comprehensive collection of data on physical properties was compiled and utilized to develop the design evaluation formulae of Monju fuel.

After development of the initial design of Monju, innovative technologies for measuring physical properties were developed. Also the role of FRs was widened from breeding to incinerating long-lived minor actinides (MAs) to reduce the volume and harmfulness of high-level radioactive waste. It was therefore important to improve the reliability and accuracy of physical property measurement and to quantitatively evaluate the effect of MAs.

The crystal of MOX fuel has a fluorite structure, and the regions with excessive oxygen (O/M ratio: larger than 2.0) and the regions with insufficient oxygen (O/M ratio: less than 2.0) can widely co-exist in a stable state. Because a slight change in O/M ratio greatly changes the fuel physical properties, accurate control of the O/M ratio is required to measure the physical properties accurately. Moreover, because of the accumulation of americium in fuel as a result of the extended shutdown of Monju, it was essential to evaluate the effect of americium on thermophysical properties such as thermal conductivity and melting point for the Safety Review for Monju restart. To address these issues, a new experimental method was developed for precisely controlling the O/M ratio in MOX fuel by adjusting the oxygen partial pressure in the

atmosphere. Using this new method, the melting point and thermal conductivity of americium-containing fuel were measured accurately. In addition, a wide variety of high-temperature physical properties, such as the oxygen potential, thermal expansion coefficient, and oxygen diffusion coefficient, were measured.

Achievements pertaining to the melting point and thermal conductivity are described below in detail.

(1) Melting point

The melting point of MOX fuel was conventionally measured using a method in which a test sample was vacuum sealed in a tungsten capsule and heated to determine the melting point based on the thermal arrest (i.e., temperature stops increasing and stays constant). It was found out, however, that the melting point of MOX fuel could not be measured accurately by this method because of the reaction between the tungsten capsule and MOX sample with a high plutonium content. To resolve this problem, a new measurement technique was developed, in which an inner vessel made of rhenium, material not reactive with MOX fuel, is used as shown in Fig. 6-7. Using this method, the melting point of MOX fuel is measured accurately while suppressing the reaction between the capsule and the sample even if the plutonium content in the MOX fuel exceeds 20

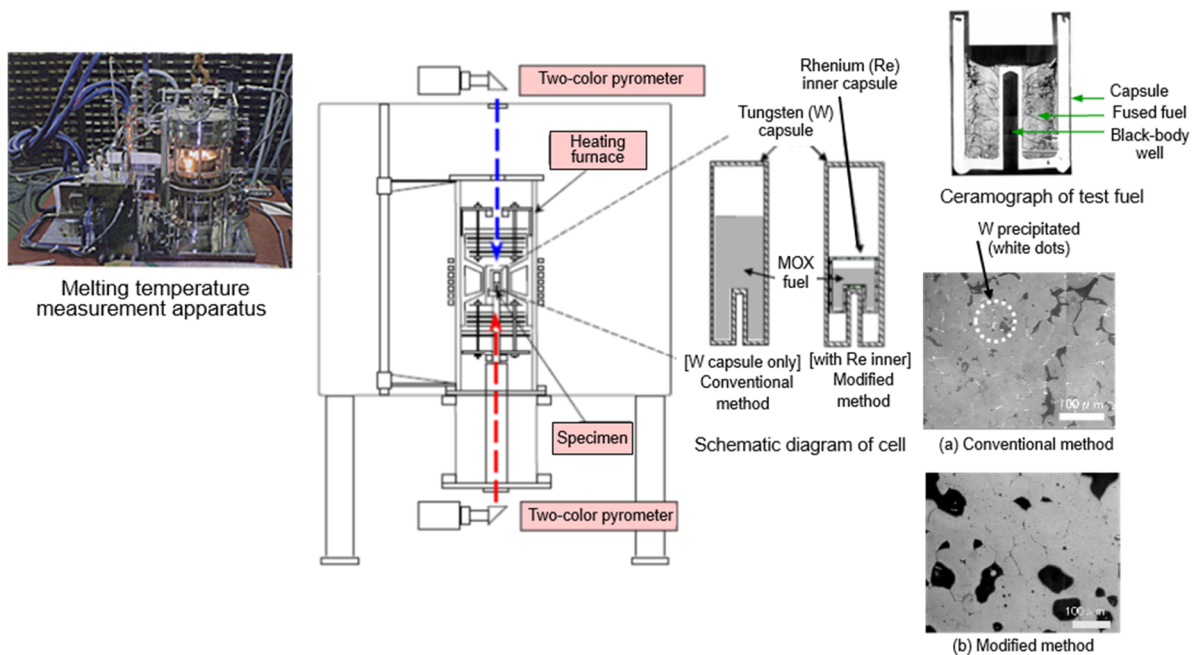


Fig.6-7 Improvement of melting point measurement for MOX fuel

6. Fuel

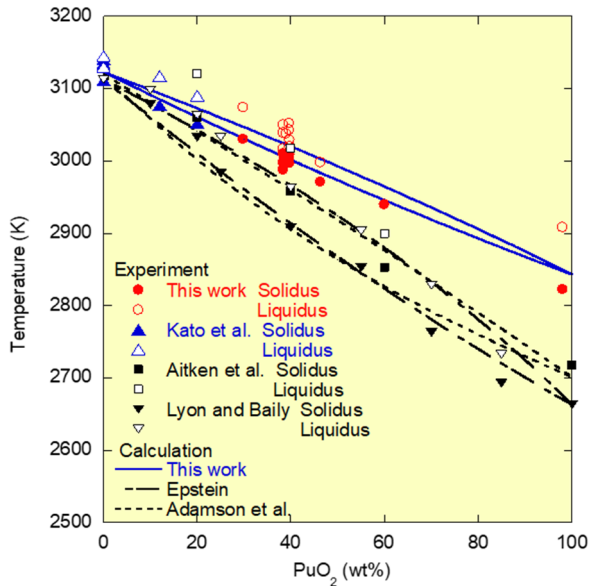


Fig.6-8 Melting points of UO_2 - PuO_2 system⁶⁻⁴⁾

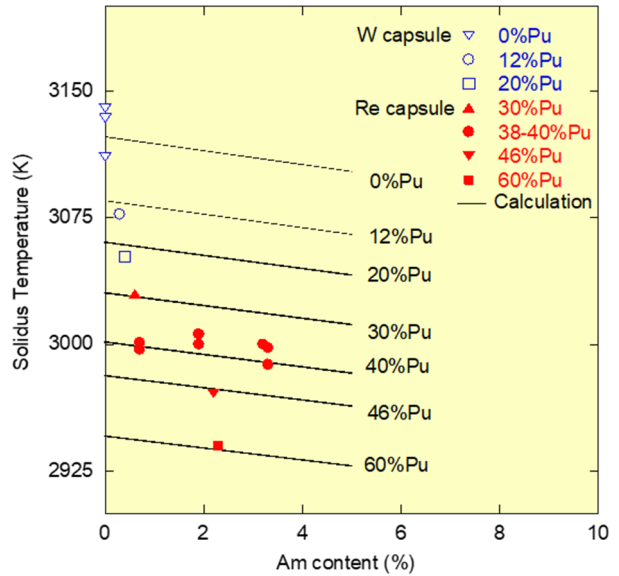


Fig.6-9 Influence of Am content on melting point⁶⁻⁴⁾

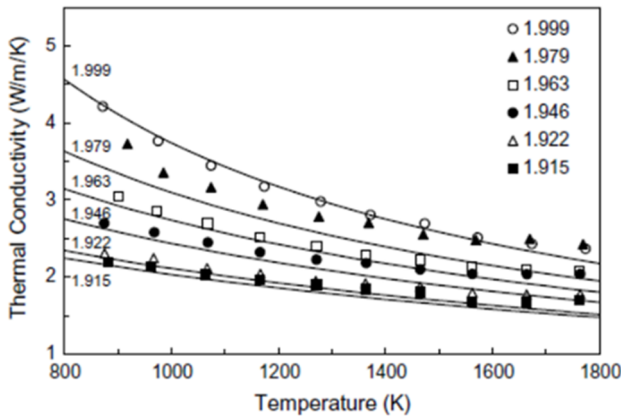


Fig.6-10 O/M dependence of thermal conductivity⁶⁻⁵⁾

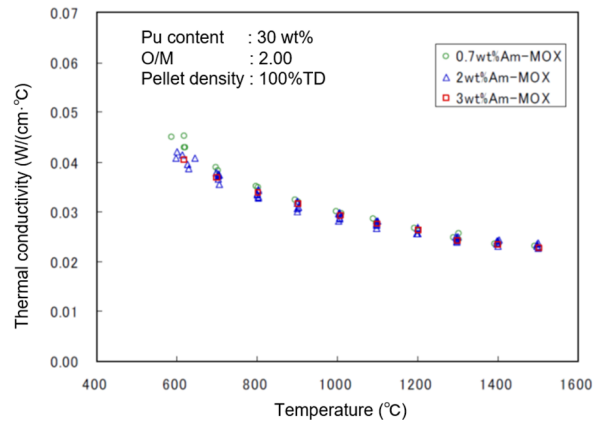


Fig.6-11 Influence of Am content on thermal conductivity⁶⁻⁶⁾

wt%. As a result, it became clear that the melting point of MOX fuel with a plutonium content of 40 wt% is higher than the previously obtained data by about 100 K, as shown in Fig. 6-8. The influence of americium content on the melting point is shown in Fig. 6-9. The melting point tends to decrease gradually with increasing the americium content. The decrease is not significant, at most 4 K for 1 wt% increase in the americium content.

(2) Thermal conductivity

In early research, the thermal conductivity of MOX fuel was measured by “the center heating method”; however, this method turned out to be unreliable with large data scattering. A new method, “the laser flash method” was later made available for measuring the thermal diffusivity, which was used to determine the thermal conductivity.

The dependence of thermal conductivity on the O/M ratio is shown in Fig. 6-10. As observed in the figure, the lower the O/M ratio, the lower the thermal conductivity. The influence of americium content on the thermal conductivity of MOX fuel is shown in Fig. 6-11.

Despite the concern that an increased americium content might significantly reduce thermal conductivity, it was confirmed that the reduction is caused by the change in the O/M ratio and that the reduction with increasing americium content is limited and does not significantly affect the fuel thermal design.

6.4 Development of high-performance SUS316-equivalent steel

The cladding requires high-temperature strength to endure the internal pressure due to

6. Fuel

The maximum values of design burnup of Monju core fuel are as follows: 94 GWd/t for the fuel subassembly, 80 GWd/t for the core-averaged subassembly at discharge, 98 GWd/t for the fuel element, and 130 GWd/t for the pellet. The maximum design fast neutron fluence is 2.3×10^{23} n/cm² (E > 0.1 MeV). Since only limited irradiation data on the cladding material were available at the time of the initial Reactor Installation Permit in 1983, it was decided to initially limit the maximum fuel subassembly burnup to 64 GWd/t (to 55 GWd/t in the core average), until irradiation data on anti-swelling properties of the 316-equivalent steel cladding could be obtained up to fast neutron fluence of 2.3×10^{23} n/cm².

For the cladding material irradiation, data for fast neutron fluence of up to 3.0×10^{23} n/cm² were obtained in the material irradiation tests (MOTA) using the U.S. FFTF. Data on fuel element and subassembly irradiation up to 1.8×10^{23} n/cm² were obtained in the Joyo MK-II core (C3M test). In the MFA-1 test at FFTF,

integrity was confirmed by irradiating fuel elements with 316-equivalent steel cladding up to 2.1×10^{23} n/cm², which was close to the target fluence.

(2) Material properties of irradiated 316-equivalent steel

a) Swelling

The fast neutron irradiation tests of cladding material were performed with an open tube (cladding specimens) as well as in a fuel element and in a fuel subassembly. This means the cladding was irradiated both with and without fuel pellets (meat) inside. A comparison of the swelling tests in FFTF between with fuel meat (fuel irradiation) and without fuel (open tube irradiation) is shown in Fig. 6-13. It was confirmed that swelling starts at lower fluence in the fuel irradiation than the open tube irradiation. This suggested that irradiation properties of the FR core materials should be demonstrated by the irradiation tests under the prototypical conditions with fuel meat⁽⁶⁻⁸⁾. It revealed that the above difference is closely related to the stability of the precipitates in the fuel irradiation. Namely, the early formation of precipitates would accelerate swelling due to temperature increase during irradiation and the early elimination of phosphides, on the contrary, would suppress swelling. This finding was reflected in the improvement of material specifications of the 316-equivalent steel. An example of PIE observation of the ultra-fine composition and crystal structures of the cladding material is shown in Photo 6-2 together with a field-emissive-type transmission electron (FE-TEM) used for elemental analysis.

b) Mechanical strength

Mechanical strength properties of 316-equivalent steel were evaluated first based on a wide range of out-of-pile and atmospheric test data obtained under various temperature conditions, followed by evaluation taking into account the in-reactor sodium environment and fast neutron fluence effects.

As already mentioned, the FR fuel element is characterized by high-temperature environment, high internal pressure due to fission gas, and large pressure differential across the cladding. It is for these characteristics that full consideration must be given to the creep damage of the cladding. For the development of the 316-equivalent steel, in-pile creep rupture data were obtained in the FFTF MOTA tests using internal-pressure-sealed cladding specimens under the actual reactor irradiation environment. It was found that the in-pile creep

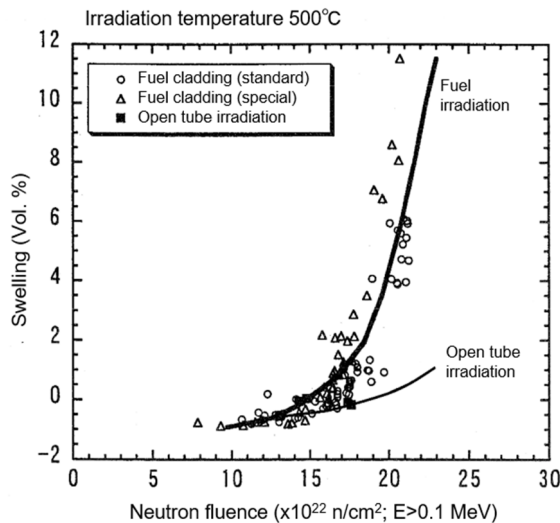


Fig.6-13 Swellings by fuel irradiation and open tube irradiation⁽⁶⁻⁸⁾

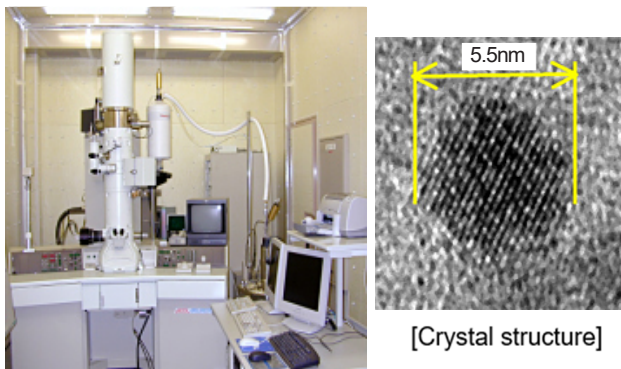


Photo 6-2 Crystal structures observed with FE-TEM

strength tended to be lower than the data in the atmosphere. This lowered creep strength was caused by: a) The recovery of the dislocations established by cold working and the coarsening of the metal carbide precipitates were promoted by neutron irradiation; and b) The minor elements such as B and P, which contributed to increasing creep strength, eluted into sodium. In the fuel design, the creep strength was conservatively set taking these into account as environmental effects.

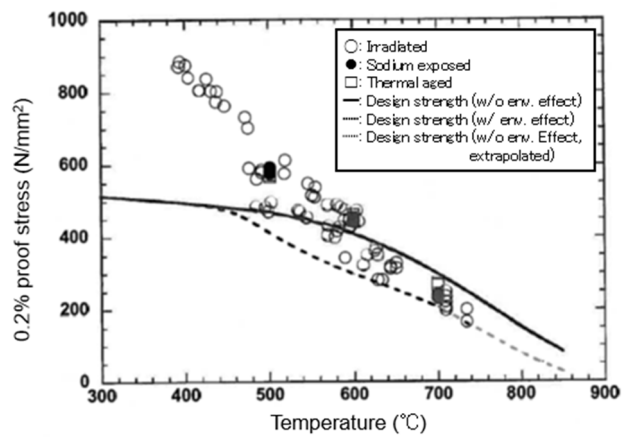
Similarly, to examine the so-called short-time strengths such as tensile strength and 0.2% proof stress, strength data were obtained (Photo 6-3) using test pieces in the atmospheric condition, as well as those after the material irradiation tests and those after removal of the fuel pellets in the PIE of the fuel element irradiation tests. Measurement data on the 0.2% proof stress and tensile strength of the 316-equivalent steel including various environmental effects are shown in Fig. 6-14.

Compared to the strength evaluation formula based on the atmospheric strength data, strength of the material influenced by the irradiation and sodium environments increases due to irradiation hardening on the low-temperature side and decreases due to carbon elution, etc. on the high-temperature side. The short-time strength of the 316-equivalent steel, however, did not exhibit prominent decrease within the range up to fast neutron fluence of $2.1 \times 10^{23} \text{ n/cm}^2$, and was confirmed to be within the acceptable range from the design perspective.

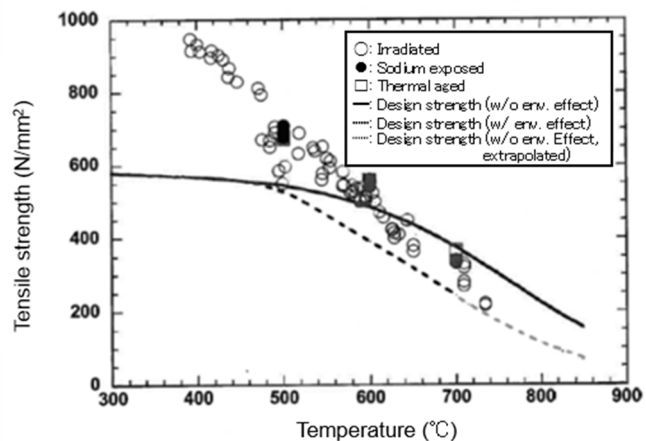
As described above, the 316-equivalent steel developed for Monju proved to satisfy the anti-swelling properties, creep rupture strength, and short-time strength required as cladding material not only in the out-of-pile tests but also through the in-pile irradiation tests with and without fuel meat.



Photo 6-3 tension testing machine



a) Temperature dependence of 0.2% proof stress



b) Temperature dependence of tensile strength

Fig.6-14 The 0.2% proof stress and tensile strength of the 316-equivalent steel

— References —

- 6-1) Inoue, M. et al., Power-to-Melts of Uranium-Plutonium Oxide Fuel Pins at a Beginning-of-Life Condition in the Experimental Fast Reactor JOYO, J. Nucl. Mater., Vol. 323, 2003, pp.108-122.
- 6-2) Tsai, H. et al., Behavior of Mixed-Oxide Fuel Elements during an Overpower Transient, J. Nucl. Mater., Vol. 204, 1993, pp.217-227.
- 6-3) Uwaba, T. et al., Study on the Mechanism of Diametral Cladding Strain and Mixed-Oxide Fuel Element Breaching in Slow-Ramp Extended Overpower Transients, J. Nucl. Mater., Vol. 429, 2012, pp.149-158.
- 6-4) Kato, M. et al., Solidus and Liquidus Temperatures in the UO_2 - PuO_2 System, J. Nucl. Mater., Vol. 373, 2008, pp.237-245.
- 6-5) Morimoto, K. et al., Thermal Conductivities of Hypo-stoichiometric (U, Pu, Am) O_{2-x} Oxide, J. Nucl. Mater., Vol. 374, 2008, pp.378-385.
- 6-6) Morimoto, K. et al., Thermal Conductivity of (U, Pu, Am) O_2 Solid Solution, J. Alloys and Compounds, Vol. 452, 2008, pp.54-60.
- 6-7) Tateishi, Y. et al., Development of Modified SUS 316 Stainless Steel as Core Material for Fast Breeder Reactors, Journal of the Atomic Energy Society of Japan, Vol. 30, No. 11, 1988, pp.1005-1019 (in Japanese).
- 6-8) Donomae, T., et al., Swelling Behavior of PNC316 Stainless Steels Cladding Tube; an Examination based on PIE Data of FFTF/MFA-1, Joyo/C3M and Joyo/B8 Irradiation Test, JNC-TN9400 2001-092, 2001, 40p (in Japanese).

